Journal of Applied Geophysics 126 (2016) 98–115

Contents lists available at ScienceDirect

Journal of Applied Geophysics

journal homepage: www.elsevier.com/locate/jappgeo

Permanent electrical resistivity measurements for monitoring water circulation in clayey landslides

J. Gance [a,c,*], J.-P. Malet [a], R. Supper [b], P. Sailhac [a], D. Ottowitz [b], B. Jochum [b]

[a] Institut de Physique du Globe de Strasbourg, CNRS UM7516, EOST/Université de Strasbourg, 5 rue Descartes, 67084 Strasbourg Cedex, France
[b] GBA, Geological Survey of Austria, Neulinggasse 38, 1030 Wien, Austria
[c] BRGM, Bureau de Recherches Géologiques et Minières, 3 Avenue Claude Guillemin, 45060 Orléans, France

ARTICLE INFO

Article history:
Received 4 June 2015
Received in revised form 5 January 2016
Accepted 15 January 2016
Available online 21 January 2016

Keywords:
Time series analysis
Electrical properties
Resistivity
Hydrogeophysics
Landslide
Fissures

ABSTRACT

Landslides developed on clay-rich slopes are controlled by the soil water regime and the groundwater circulation. Spatially-distributed and high frequency observations of these hydrological processes are important for improving our understanding and prediction of landslide triggering. This work presents observed changes in electrical resistivity monitored at the Super-Sauze clayey landslide with the GEOMON ^{4D} resistivity instrument installed permanently on-site for a period of one year. A methodological framework for processing the raw measurement is proposed. It includes the filtering of the resistivity dataset, the correction of the effects of non-hydrological factors (sensitivity of the device, sensitivity to soil temperature and fluid conductivity, presence of fissures in the topsoil) on the filtered resistivity values. The interpretation is based on a statistical analysis to define possible relationships between the rainfall characteristics, the soil hydrological observations and the soil electrical resistivity response. During the monitoring period, no significant relationships between the electrical response and the measured hydrological parameters are evidenced. We discuss the limitations of the method due to the effect of heat exchange between the groundwater, the vadose zone water and the rainwater that hides the variations of resistivity due to variations of the soil water content. We demonstrate that despite the absence of hydrogeophysical information for the vadose zone, the sensitivity of electrical resistivity monitoring to temperature variations allows imaging water fluxes in the saturated zone and highlighting the existence of matrix and preferential flows that does not occur at the same time and for the same duration. We conclude on the necessity to combine electrical resistivity measurements with distributed soil temperature measurements.

1. Introduction

Water circulation within a slope, in both the saturated and unsaturated zones, is one of the most common controlling factors of landslide first time failures or reactivation (Van Asch et al., 1999; Malet et al., 2005b). The internal structure and geometry, petrophysical properties and the elementary hydrological processes govern the spatial and temporal variations of water storage in a slope. The hydrological models generally used for slope stability analysis which reasonably well incorporate pore water pressure increase or matric suction decrease are not always able to explain sharp variations of the groundwater level, especially for clayey slopes. The incorporation of other important elementary hydrological processes (Fig. 1) such as dynamic preferential flows linked to soil heterogeneity or to the presence of fissures (Van Asch et al., 1999), water storage and circulation in the vadose zone (Bogaard and Van Asch, 2002; Philip, 1991), or the presence of local perched water tables (Van Asch and Buma, 1997) to name a few, still lags behind because of a lack of knowledge on these processes at the field scale.

In this context, hydrogeophysical monitoring of water storages and fluxes is interesting for understanding landslide hydrology because of its sensitiveness to water content changes in the subsurface and because it provides spatially distributed images of the petrophysical parameters. Time-lapse Electrical Resistivity Tomography (ERT) is often used to detect, map and track water circulation in the subsoil (Revil et al., 2012) and is able to complement point-based observations (Miller et al., 2008). Recently, several automated monitoring instruments, specifically developed for long-term time-lapse resistivity monitoring in rugged slope conditions, have been developed, such as the ALERT system, (Kuras et al., 2009; Wilkinson et al., 2010), the GEOMON ^{4D} system (Supper et al., 2008, 2014) and the A-ERT system (Hilbich et al., 2011). Up to now, only few studies are discussing the processing of time series of resistivity datasets acquired on landslides and the extraction of useful information for understanding slope hydrology (Perrone et al., 2014).

Lebourg et al. (2005) repeated five ERT measurements on a profile located at the La Clapière (southeast France) rocky landslide. The results are compared to water flow rates estimated from groundwater

* Corresponding author at: Institut de Physique du Globe de Strasbourg, CNRS UM7516, EOST/Université de Strasbourg, 5 rue Descartes, 67084 Strasbourg Cedex, France.
E-mail address: jgance@unsitra.fr (J. Gance).

http://dx.doi.org/10.1016/j.jappgeo.2016.01.011
0926-9851/

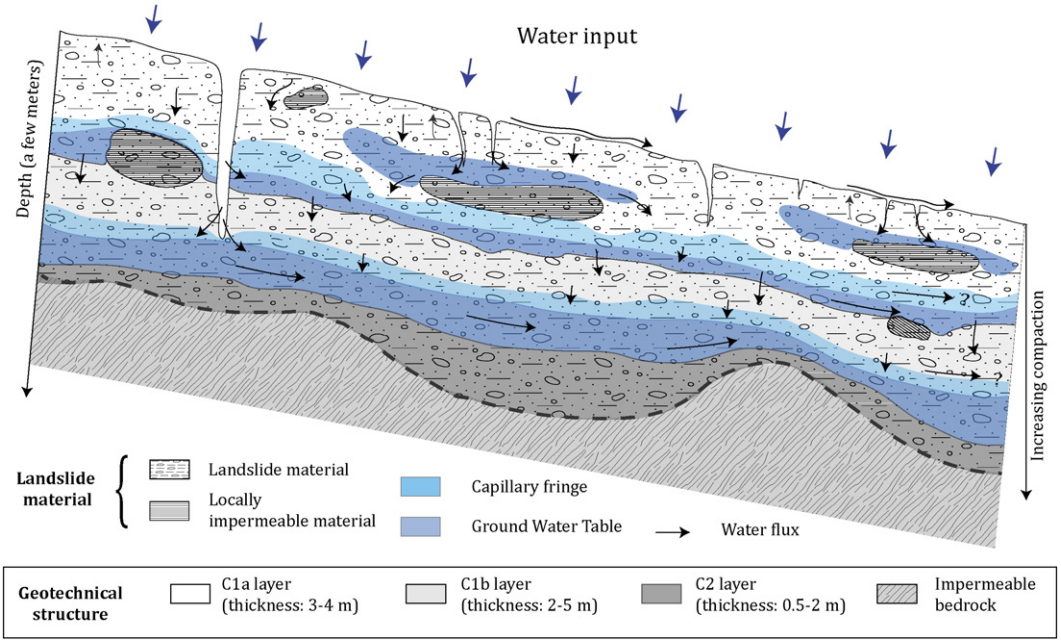

Fig. 1. Water storages and fluxes in clayey landslide body characterized by complex soil structures (macroporosity, stratified aquifers), lateral and vertical variations in soil properties (porosity, density, hydraulic permeability) and the presence of local water barriers (impermeable blocks, bedrock). The different types of water fluxes are indicated in the figure as a response of the slope to a rain or a snowmelt event. The geotechnical structure given by the C1a, C1b, C2 layers and the substratum is also indicated by different colors.

chemical analysis. At the same landslide, Jomard et al. (2007) performed a 12 h continuous ERT measurements during a controlled infiltration experiment over a period of 300 min and highlighted the presence of deep cracks contributing to a direct percolation of the surface water in depth. Lebourg et al. (2010) performed a time-lapse ERT survey at the Vence landslide (southeast France) for three months and identified the existence of two types of hydrological responses of the subsoil to rainfall events from the analysis of inverted resistivity. At the Avignonet clayey landslide (Eastern France), Bièvre et al. (2012) repeated campaigns of electrical resistivity measurements along a profile for a period of two years and observed anomalies of resistivity around large fissures suggesting that they constitute preferential water pathways. Travelletti et al. (2012b) used time-lapse ERT to characterize the spatial and temporal development of water circulation at the Laval–Draix clayey landslide (Southeast France) during a controlled infiltration experiment over a plot of 100 m^2. At the start of the experiment, the soil was in nearly unsaturated conditions. Sprinklers were used to infiltrate a water containing chemical tracers. Water infiltration was monitored with time-lapse ERT repeated every 3 h during 67 h. The analysis of the resistivity variation in space and time allowed proposing a conceptual model of infiltration integrating preferential lateral flows in fissures and around impermeable blocks. The inverted resistivity

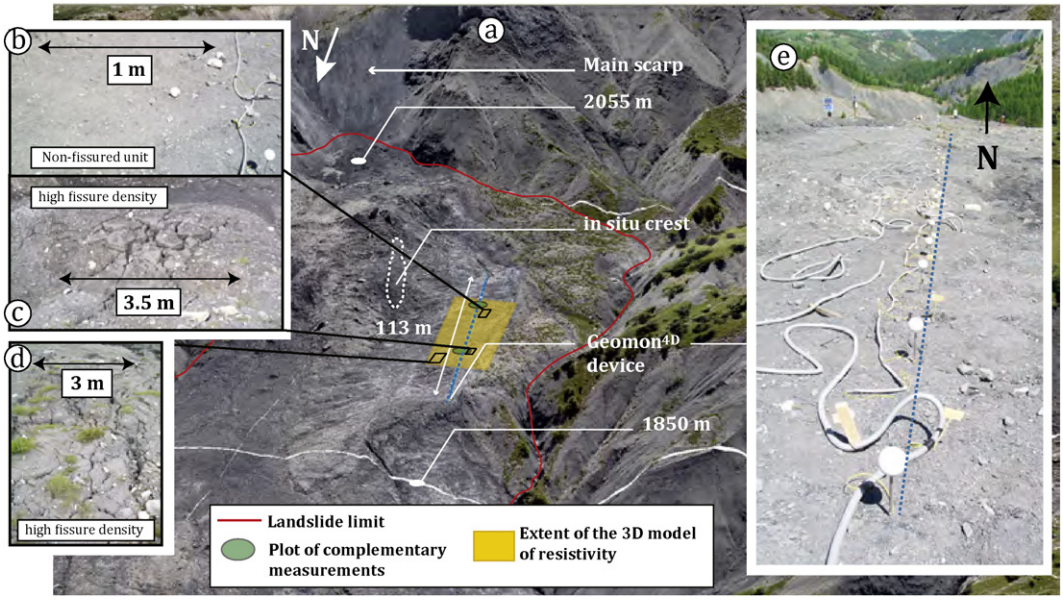

Fig. 2. Location of the GEOMON ^{4D} profile and of the plots of complementary measurements on the Super-Sauze landslide. The profile crosses several areas with different soil surface characteristics.

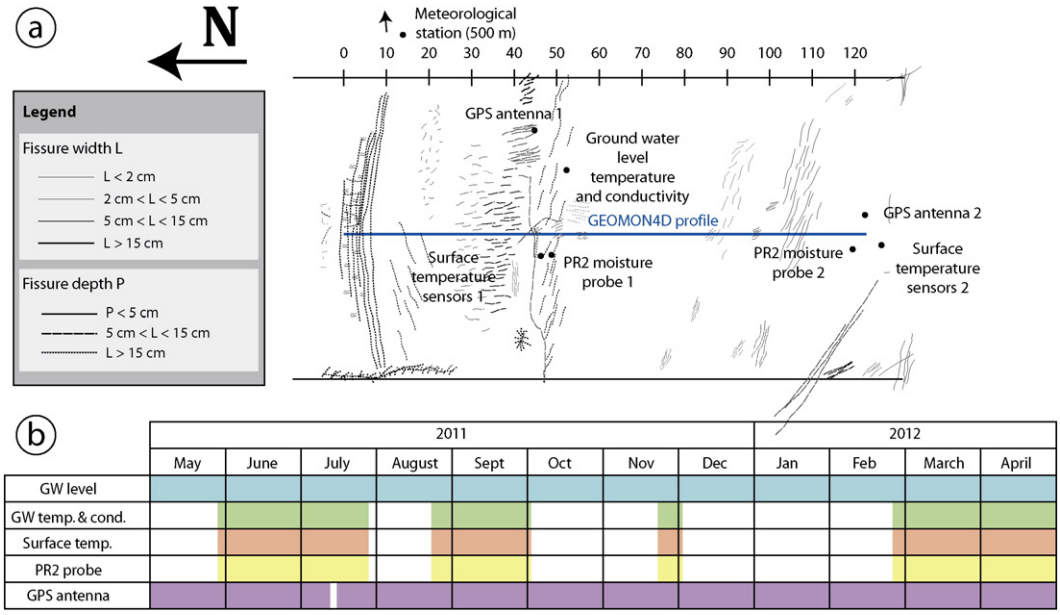

Fig. 3. Complementary metrology to the ERT measurement: a) location of the different sensors on the map of surface fissures surveyed in May 2011 during the installation and b) table resuming the data available during the monitoring period.

values are interpreted in terms of steady-state flow conditions and apparent hydraulic permeabilities of the soil are estimated. A similar experiment was carried out by Lehmann et al. (2013) who monitored electrical resistivity at the Rüdlingen landslide (Northern Switzerland) for a period of 64 h, and identified the spatial and temporal evolution of the wetting front in response to hydrological perturbations. Finally, Luongo et al. (2012) analyzed the variations of electrical resistivity on a landslide in the Basilicata region (Southern Italy) for a period of two years. The authors highlighted the long term stability of the apparent resistivity signal and established correlations between electrical resistivity and soil moisture for the subsoil. These limited number of experiments highlighted the complexity of interpreting time-lapse ERT datasets on landslides. Most of the time, the interpretation of the resistivity values in terms of hydrological knowledge is limited to the mapping of resistivity anomalies or to the establishment of site-dependent statistical relationships among resistivity and soil moisture. The quantitative interpretation of large resistivity datasets acquired is very difficult because of various slope conditions (saturated versus unsaturated media, complex slope structures), changing petrophysical and hydrological parameters of the soil (porosity, density, permeability, temperature), of the fluid (conductivity, temperature) in space and time, and changes in the instrument acquisition geometry because of the movement of the electrodes.

The objectives of this work are 1) to estimate the contribution of several non-hydrological factors on the resistivity values in order to define the 'real' hydrological signal of the slope, 2) to interpret qualitatively the electrical responses measured after significant rainfall events and 3) to identify statistical relationships between the electrical responses of the slope and the rainfall event characteristics. The experimental dataset consists of one year of electrical resistivity measurements acquired on a longitudinal profile at the clayey Super-Sauze landslide (Southeast France).

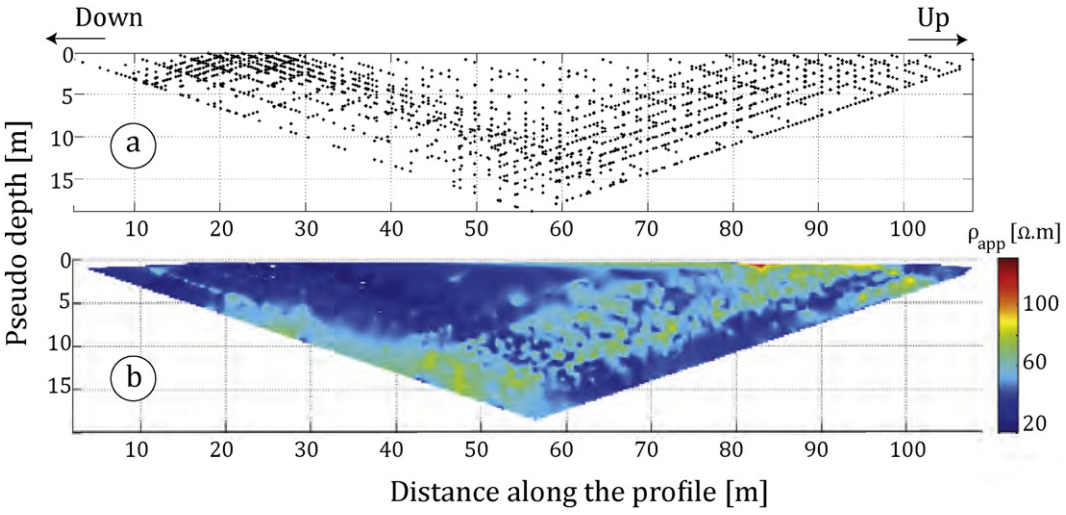

Fig. 4. Representation of data on pseudo-section of apparent resistivity: a) location of the measurement points and b) example of an interpolated pseudo-section of apparent resistivity measured on the 31 May 2011.

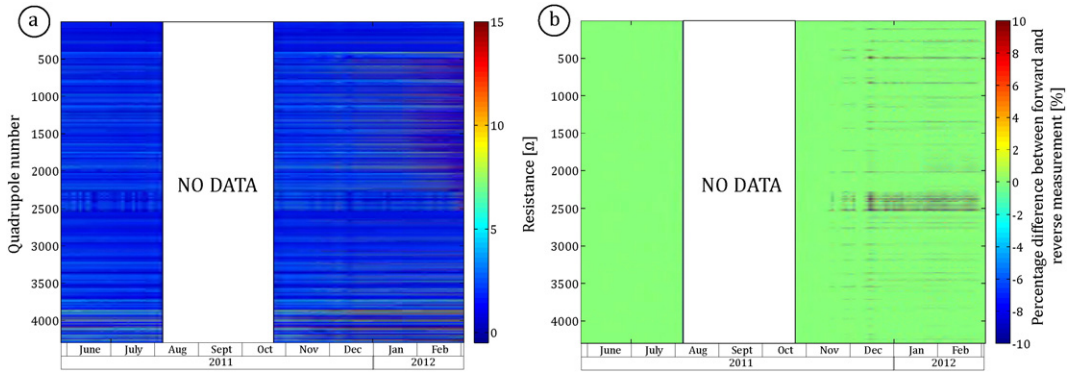

Fig. 5. Raw data example: a) Mean between forward and reverse resistances for each quadrupole with time; b) relative difference between forward and reverse resistances with time.

2. Study site and monitoring instruments

2.1. Study site

The experiment has been carried out at the Super-Sauze landslide (Barcelonnette Basin, Southeast French Alps). The landslide, which has developed in weathered Callovo-Ofxordian black marls, is active since the beginning of the 1960s. In 2014, the landslide extents over a horizontal distance of 880 m and occurs between elevations of 2105 m at the crown and 1760 m at the toe with an average 25 slope gradient. The total volume is estimated at 750,000 m^3. The landslide is bordered by two lateral streams draining the groundwater table. Its dynamics is controlled by bedrock geometry (Travelletti and Malet, 2012; Gance et al., 2014), rock mass fabric and hydrology (Malet et al., 2005a). Morphological features induced by the sliding and flowing mode of the landslide are easily recognizable at the surface with the presence of lobes, boulders and fissures at different locations (Stumpf et al., 2013). The landslide is continuously active with average displacement rates in the range of 0.05 to 0.20 m day^{-1} (Malet et al., 2005b). Landslide surges (acceleration and/or fluidization) consecutive to large rainfall events or to a sudden melting of the snowcover have been observed in the past with average displacement rates of several meters per day (Travelletti et al., 2012a). These surges are difficult to forecast but are controlled by the water circulation and the

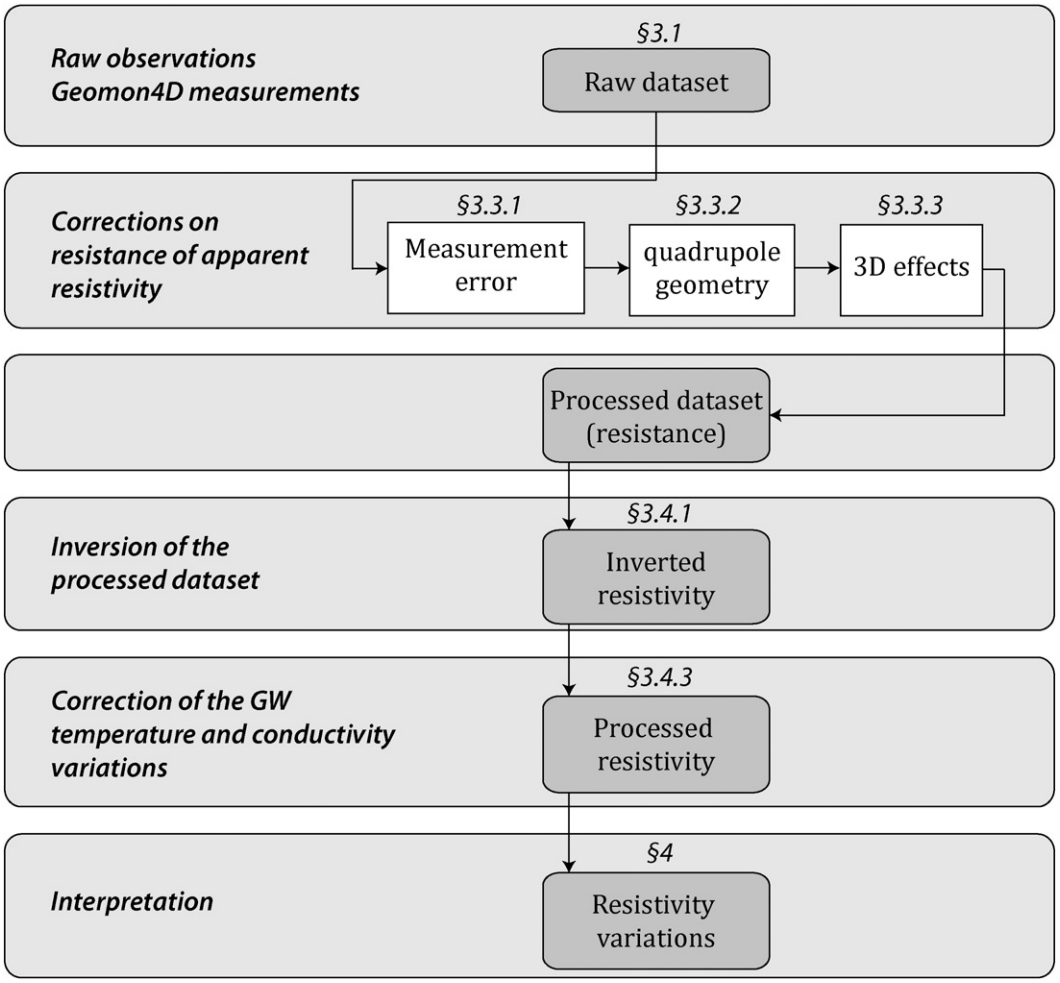

Fig. 6. Methodological flowchart used in this study.

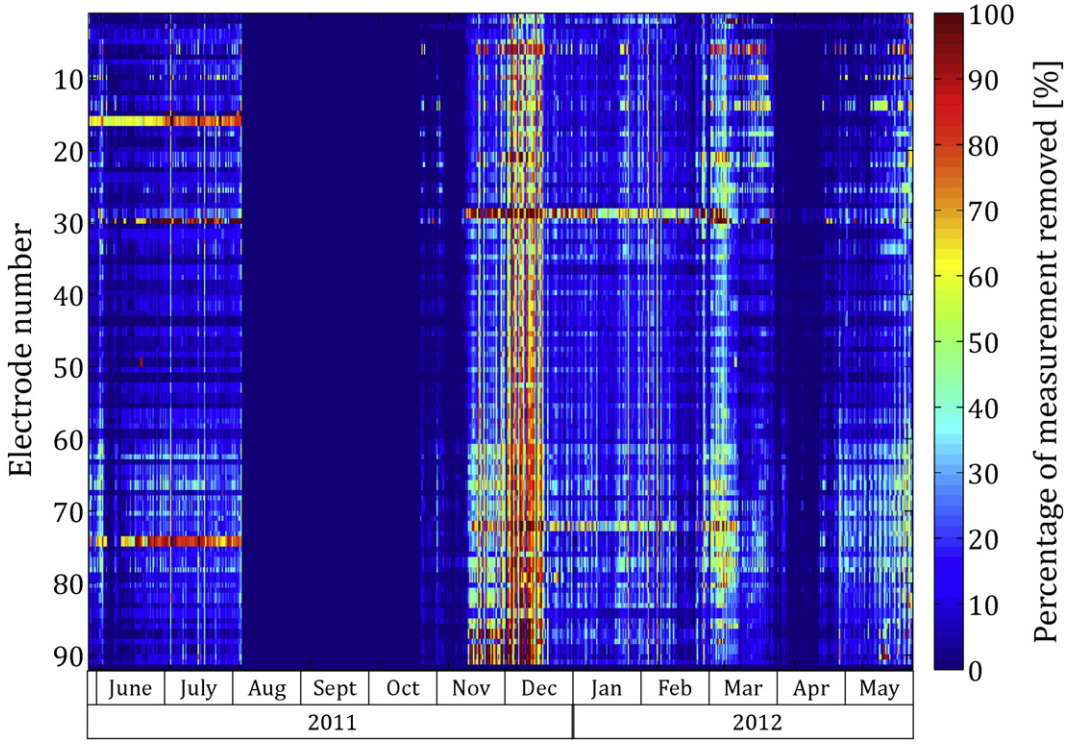

Fig. 7. Percentage of measurements removed per electrode after the correction of the errors of measurement.

development of excess pore water pressures (Malet et al., 2005b). The hydrological response of the slope to rain or snowmelt events is non-linear and depends of the volume of infiltrating water, the position of the groundwater table, the amount of water stored in the vadose zone and the properties of the soil surface with the presence of fissures or structural/sedimentary crusts (Malet et al., 2003; Montety et al., 2007; Krzeminska et al., 2013; Malet and Maquaire, 2004).

The geotechnical model of the landslide consists of two layers lying on a impermeable bedrock (S) made of in-situ black marls. The upper C1 layer is composed of weathered black marls in movement. This unit is divided in two sub-units C1a and C1b with different geotechnical parameters. The C2 layer describes of a compacted layer of reworked black marls called 'dead-body'. It is considered as impermeable (permeability of 10^{-8} m s $^{-1}$) and (with displacement rates of less than ≤0.1 mm year^{-1}, Maquaire et al., 2001). The resistivity measurements previously carried out on the landslide (Grandjean et al., 2006, 2007; Travelletti and Malet, 2012) show that a significant contrast of resistivity is observed between C2 (≤50 Ω · m) and the bedrock (≥50 Ω · m) while the resistivity in the landslide material (C1 and C2) increases linearly with depth, so that the limits between C1a, C1b and C2 are not detectable.

The reworked black marls layers (C1 and C2) have a low resistivity explained by a clay fraction greater than 20% and by highly mineralized ground waters (2650 $\mu S \cdot cm^{-1}$ in average, Debieche et al., 2012). Added, to the nearly saturated conditions for most landslide parts over the year, the expected percentage of variation of resistivity resulting from an increase of water content is therefore small (e.g. only a few percent). Moreover, the accurate measurement and processing of electrical resistivity on this type of soil is difficult because of the heterogeneity of the soil material (presence of blocks, of surface fissures, spatial variation of grain size and of clay content) and because of complex monitoring conditions due to high surface displacement rates. In this context, the detection of weak changes in resistivity in space and time is challenging.

2.2. Characteristics of the GEOMON ^{4D} measurement device

We installed the GEOMON ^{4D} measurement instrument on a longitudinal profile located in the upper part of the landslide in an area characterized by contrasting soil units (in terms of density of surface fissures and surface grain sizes, Fig. 2) and by the presence of a shallow groundwater table (located on average at −1.5 m from the surface). The objective was to investigate the contributions of these soil units to localized spatial variations in infiltration rates in the topsoil (0–1 m).

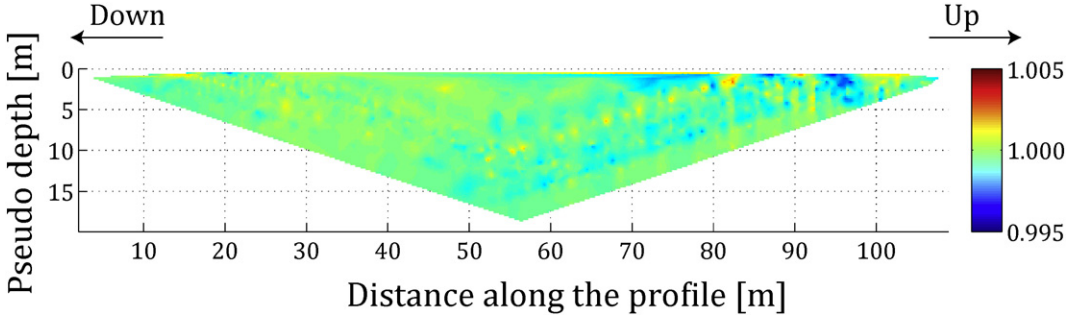

Fig. 8. Pseudo section of correction factor C_f applied on the raw resistances.

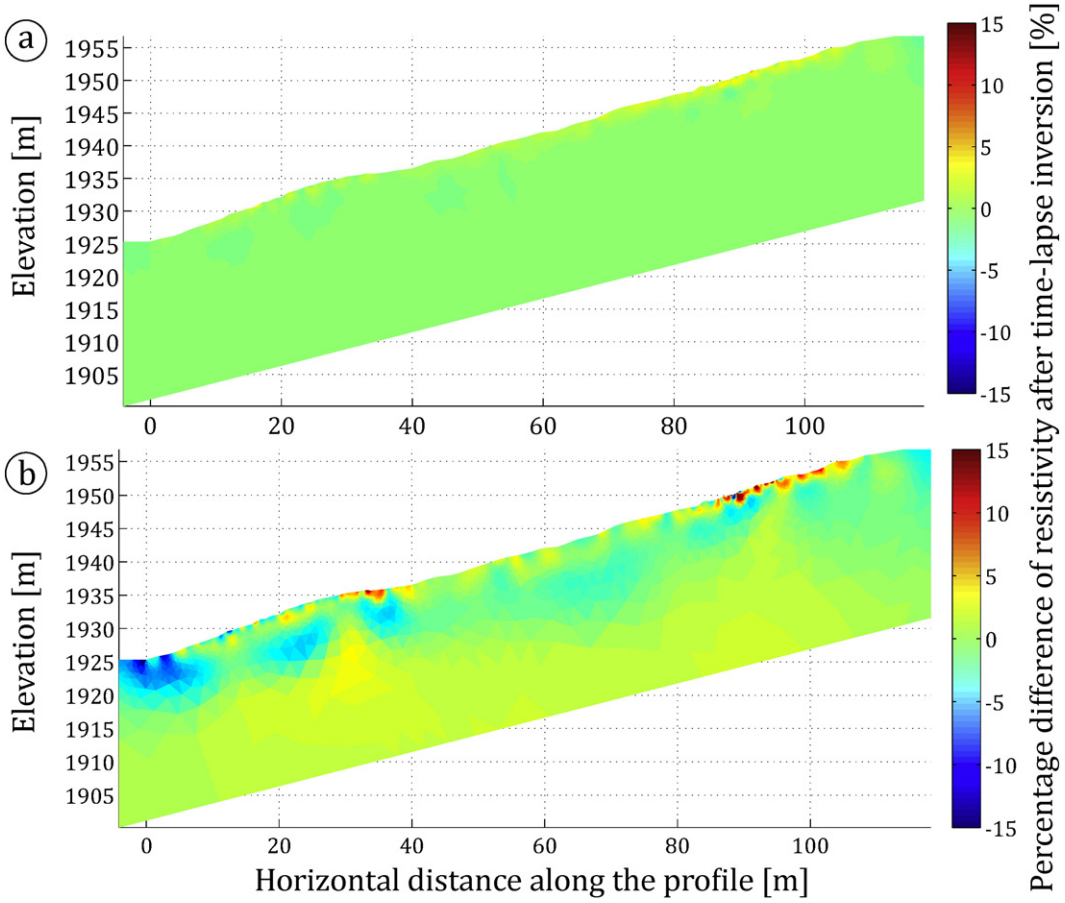

Fig. 9. Example of correction of the electrode movement for a time-lapse inversion: a) percentage difference of the time-lapse inverted datasets of the 27th and 29th May 2011 without considering electrode movement and b) when correcting for the electrode movement.

The GEOMON ^{4D} resistivimeter has been developed by the Geological Survey of Austria (GSA, Supper et al., 2002; Supper and Roemer, 2003, 2004). The system is able to measure soil electrical resistivity and self-potential and is characterized by a flexible architecture allowing the installation of any number of current and potential electrodes. The main characteristics of the system are a high speed of acquisition (which approximatively equals 3000 measurements per hour in single channel mode) and the recording of the full electrical signal. During an acquisition, the voltage is continuously measured with a sampling rate of 500 values per second (during 0.2 s) allowing to precisely control the data quality. For each quadrupole, forward and reverse measurements (for which only the injection electrodes are swapped; the measurement electrodes are unchanged) are performed. This procedure allows for quantifying the error repeatability.

The device used at Super-Sauze is constituted of 93 steel electrodes separated in 24 current injection and 69 potential measurement electrodes, with a total length of 113 m. In this experiment, the electrode spacing is variable and customized according to the soil surface properties. An electrode spacing of respectively 0.5 m, 1.0 m and 2.0 m has been used for soil units affected by respectively a low fissure density (average of 2.2 m m $^{-2}$), a high fissure density (average of 3.8 m m $^{-2}$) and the absence of fissures. We choose these different electrode spacings to be able to track the expected surficial preferential flows in the fissured areas.

Table 1
RMS errors for the 2D inverted profiles.

Profile	P1	P2	P3	P4	P5	P6	P7	P8
RMS error [%]	4.01	3.97	5.95	5.74	5.70	4.77	6.08	4.40

The monitoring system has been installed in May 2011. The GEOMON ^{4D} is powered by a 235 W solar panel and a methanol fuel cell (SFC efoy Pro600) combined with appropriate batteries for energy storage. The data are transferred daily by GSM to the research institutes. Two measurements of resistance are performed daily (at 0:00 and 12:00 GMT) with a sequence of 4300 quadrupoles according to a multiple gradient array. The entire measurement takes approximately 1 h. This resistivity array has been chosen because it allows exploiting the multichannel capability of the GEOMON ^{4D} and provides better resolutions than other usual resistivity arrays while maintaining a good signal to noise ratio (Dahlin and Zhou, 2004, 2006). This resistivity array is also adapted to measurements in complex media (fissures, blocks) and is able to image structures of different orientations. The Depth of Investigation Characteristic (DIC) functions, computed for each quadrupole with the Bhattacharya and Dutta method (Bhattacharya and Dutta, 1982) for a homogeneous medium, ranges between 0.5 and 11.5 m for a mean DIC of 4.7 m.

Several point-based hydrological sensors were installed to complement the GEOMON ^{4D} system at two plots located upslope and downslope of the profile (Fig. 3a). The sensors are a groundwater level sensor (Campbell CS450), a water temperature and conductivity sensor (Campbell CS547A), and soil temperature sensors (Campbell PT105E) installed at depths of −0.1, −0.2 and −0.3 m. Meteorological parameters (rainfall, air temperature, wind velocity and direction, relative air humidity, net radiation) are monitored at a distance of 500 m from the profile on a stable slope. The displacements of the electrodes are monitored by campaigns of double difference differential GPS and by terrestrial optical cameras (Gance et al., 2014).

The apparent resistivity can be plotted as a pseudo-section, with a pseudo-depth computed from the formula of Dahlin and Zhou (2006).

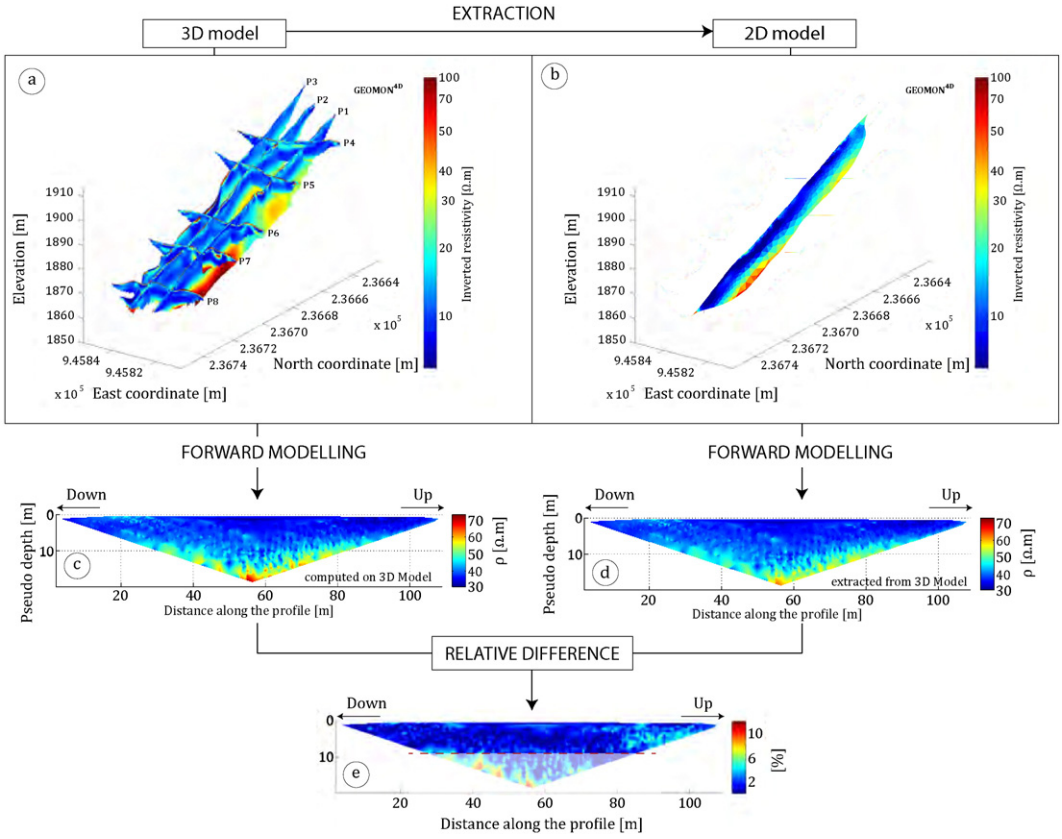

Fig. 10. Correction of the 3D effects on 2D measurement profiles. a) 3D representation of the 8 tomograms used to construct a pseudo 3D model by interpolation. b) 2D resistivity profile extracted from the 3D model at the location of the GEOMON^{4D} c) apparent resistivity pseudo-section calculated on the 3D model, d) apparent resistivity pseudo-section calculated on the 2D model extracted from the 3D model; e) Percentage difference between a) and b). The largest differences are identified for large pseudo-depths. The removing of data characterized by pseudo-depths greater than 9 m limits the 3D effects amplitude below 5%.

The point measurement locations are presented in Fig. 4a and an example of interpolated apparent resistivity pseudo-section is presented in Fig. 4b. Due to the different electrode spacings, the coverage with pseudo-depths is not identical for all abscissa.

3. Data processing methodology

3.1. Electrical resistivity dataset: data quality

The raw data are the injected current i, the total voltage V^T and the self-potential for forward and reverse measurements. A mean resistance is calculated with Eq. (1) where V_f and V_r are respectively the forward and reverse voltages subtracted from the self-potential. The resistance and the relative difference between forward and reverse resistances measured during approximately one year are presented in Fig. 5.

$$R = \frac{1}{2}\cdot\left(\frac{V_f}{I_f} + \frac{V_r}{I_r}\right) \quad (1)$$

From the 1st August 2011, 2 months after its setup, the GEOMON^{4D} is out of order for 3 months because of lightning. The 26th of October 2011, the GEOMON^{4D} as been repaired. During the winter period, soil freezing creates large differences between forward and reverse resistances indicating weak repeatability of the measurements possibly due to poorer soil/electrode contacts (Fig. 7). Thereby, for this study, we chose to interpret only the first period between the 27th of May and the 27th of July 2011 when the resistance measured for each quadrupole with time is relatively stable with a low percentage difference between forward and reverse resistances (≤1%) and where the complementary non-geophysical data are available (Fig. 3b). Other periods characterized by small relative difference exist during the winter period when the landslide is covered of snow but when we do not expect significant hydrological processes.

3.2. Contribution of terms to the resistivity signal

A rapid processing of the time-lapse resistivity data would assume that the soil electrical resistivity variations are only created by variation of the soil water content. However, the soil electrical resistivity is controlled by many other non-hydrological factors whose effect can be non-neglible for landslide study, such as:

- the existence of instrumental noise and measurements errors (Peter-Borie, 2011);
- the presence of 3D effects on 2D monitoring surveys (Panissod et al., 2001; Dahlin, 1996);
- the movement of the electrodes (Uhlemann et al., 2015);
- the compression/dilatation of the media with the soil dynamic;
- the variation of the topsoil temperature (from the surface to the vadose zone);
- the variation of the groundwater temperature and conductivity (Chambers et al., 2014);
- the existence of surface heterogeneities such as surface fissures and blocks (Tabbagh et al., 2007).

The processing strategy used in this work to correct the effects of some of these factors on soil electrical resistivity, either on the raw data (resistance or apparent resistivity) or on the inverted resistivity, is presented in Fig. 6.

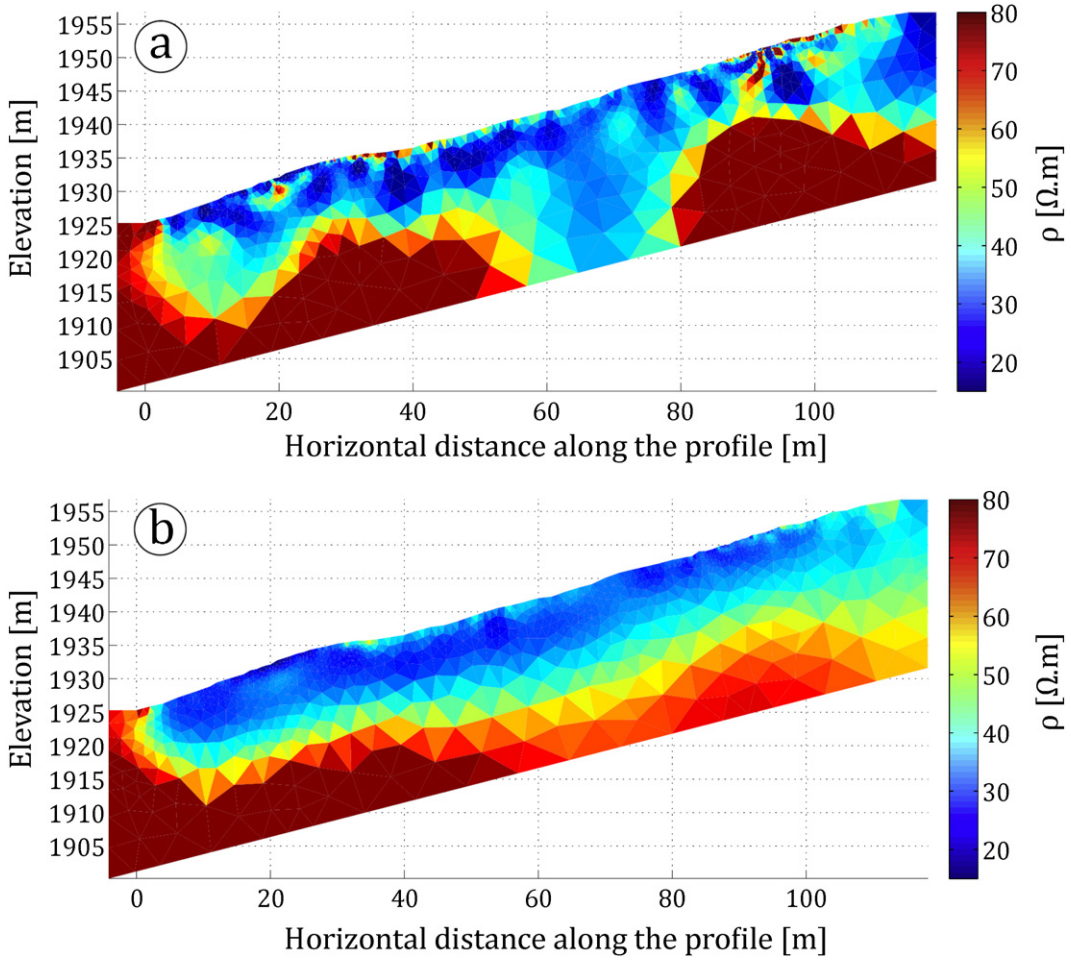

Fig. 11. Quality of the inversion of the resistivity a) inverted from the raw dataset (4300 measurements) and b) from the processed dataset (3287 measurements).

3.3. Correction on the raw dataset

3.3.1. Correction of measurement errors

In this study, the position of the electrodes has changed over time, and consequently the contact between the soil and the electrode is also changing during the period. Consequently, a part of the data present an erratic behavior characterized by localized very large resistivity variation with time and/or high frequency variations between two acquisitions. The classical filtering of measurement errors, based on a threshold on the standard deviation of the measurements (Peter-Borie, 2011; Travelletti et al., 2012b) is therefore not efficient, and we proposed to filter the data according to three criteria.

The first criterion is based on physical parameters measured during the acquisition, such as:

- the measured voltages (V_r and V_f) must be greater than 0.5 mV to ensure that the measurement is not part of the ambient noise;
- the percentage difference between forward and reverse measured resistances must be lower than 5%, in order to keep only measurement characterized by a good repeatability;
- the resistance must be positive and not equal to 0 Ω.

The second criterion selects the remaining outliers on the basis of the Probability Density Function (PDF) computed for each quadrupole on the apparent resistivity. We removed resistivity values with a probability lower than 1/50 of the maximal PDF value.

The third criterion corresponds to a high data misfit after a first independent inversion of each dataset. The data characterized by a misfit higher than 10% were removed.

The percentage of removed measurements per electrode is plotted in Fig. 7. Three electrodes (# 16, 29 and 75) are characterized by a percentage of removed measurements greater than 80% during the monitoring period. These electrodes globally show a decrease of the measurement quality in time, possibly indicating problems of contact with the soil. They are all located on landslide fissured areas. Except for these electrodes, most of the removed measurements are only for specific dates, particularly during the month of December 2011 when the soil is frozen.

3.3.2. Correction of changes in quadrupole geometry induced by electrode movement

In most ERT monitoring studies, the electrode position is fixed and the geometrical factor k computed from the electrode position is invariant in time (Kuras et al., 2009; Arora and Ahmed, 2011; Robert et al., 2012). However, for the case of landslide monitoring, the electrode movement affects the geometrical factor, especially when the landslide movement is not only a translation. As a consequence, the computation of the apparent resistivity requires the exact position of the electrodes at each measurement time. Wilkinson et al. (2010)

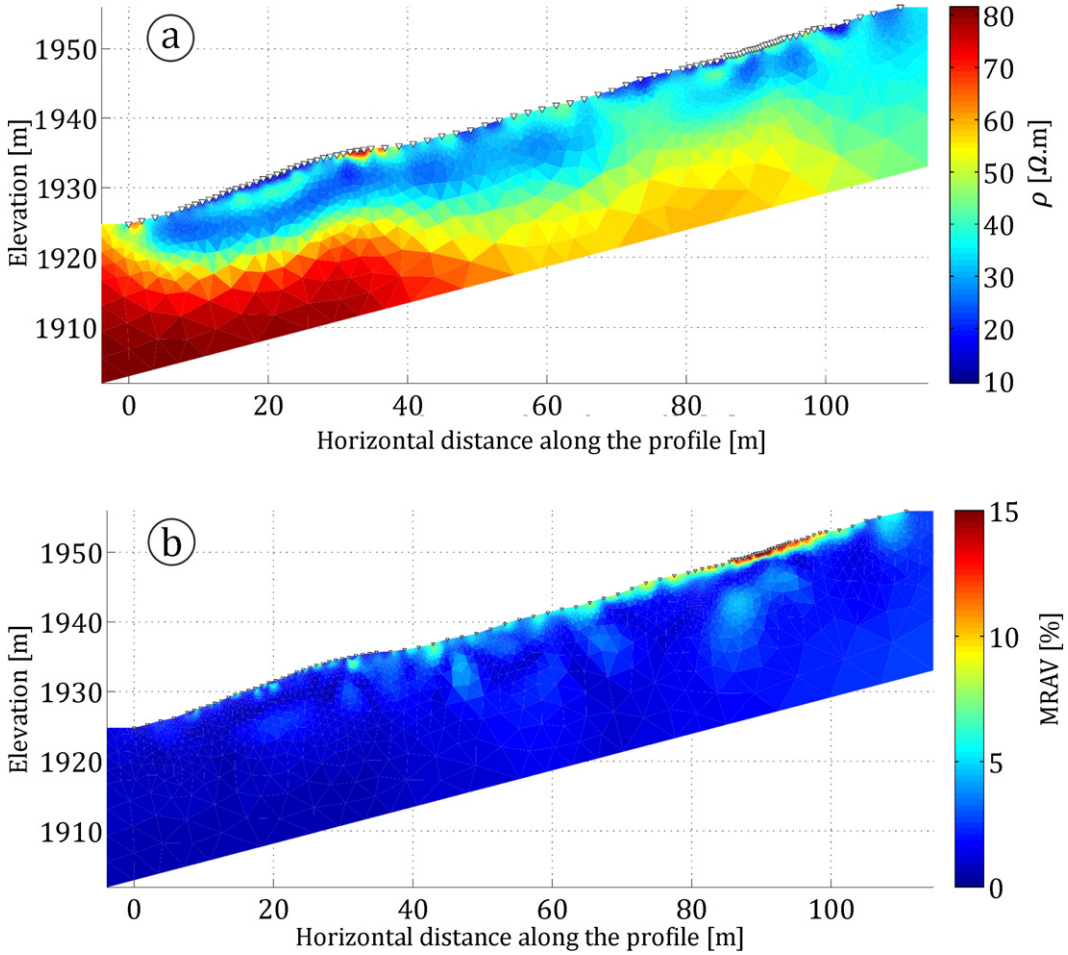

Fig. 12. Description of the reference model: a) Reference model calculated as the median resistivity of all the tomograms for the subset period 4–29 April 2012, b) percentage of maximal relative amplitude variation (MRAV) of the model or the subset period 4–29 April 2012.

handle this problem on a very slow-moving landslide by recovering electrode displacements from the ratio of apparent resistivity between two different dates.

To measure the electrode displacement, all the 24 injection electrodes were equipped of white Styrofoam spheres and their position was monitored by stereo-photogrammetry (Gance et al., 2014). The technique allows for estimating electrode positions with a minimal accuracy of 0.05 m. We correct for the electrode displacement by applying a correction factor C_f on the raw resistance such as the apparent resistivity ρ_{app} is computed according Eq. (2).

$$\begin{aligned} \rho_{app} &= k_{ref} \times C_f \times R \\ Cf &= \frac{k_t}{k_{ref}} \end{aligned} \tag{2}$$

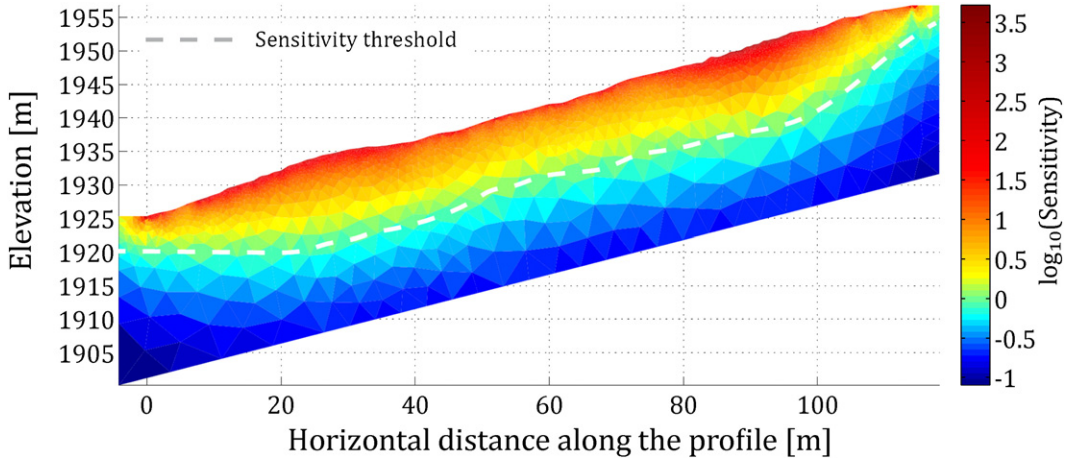

Fig. 13. Sensitivity of the inverted tomograms: logarithm of the coverage of the first inverted tomogram.

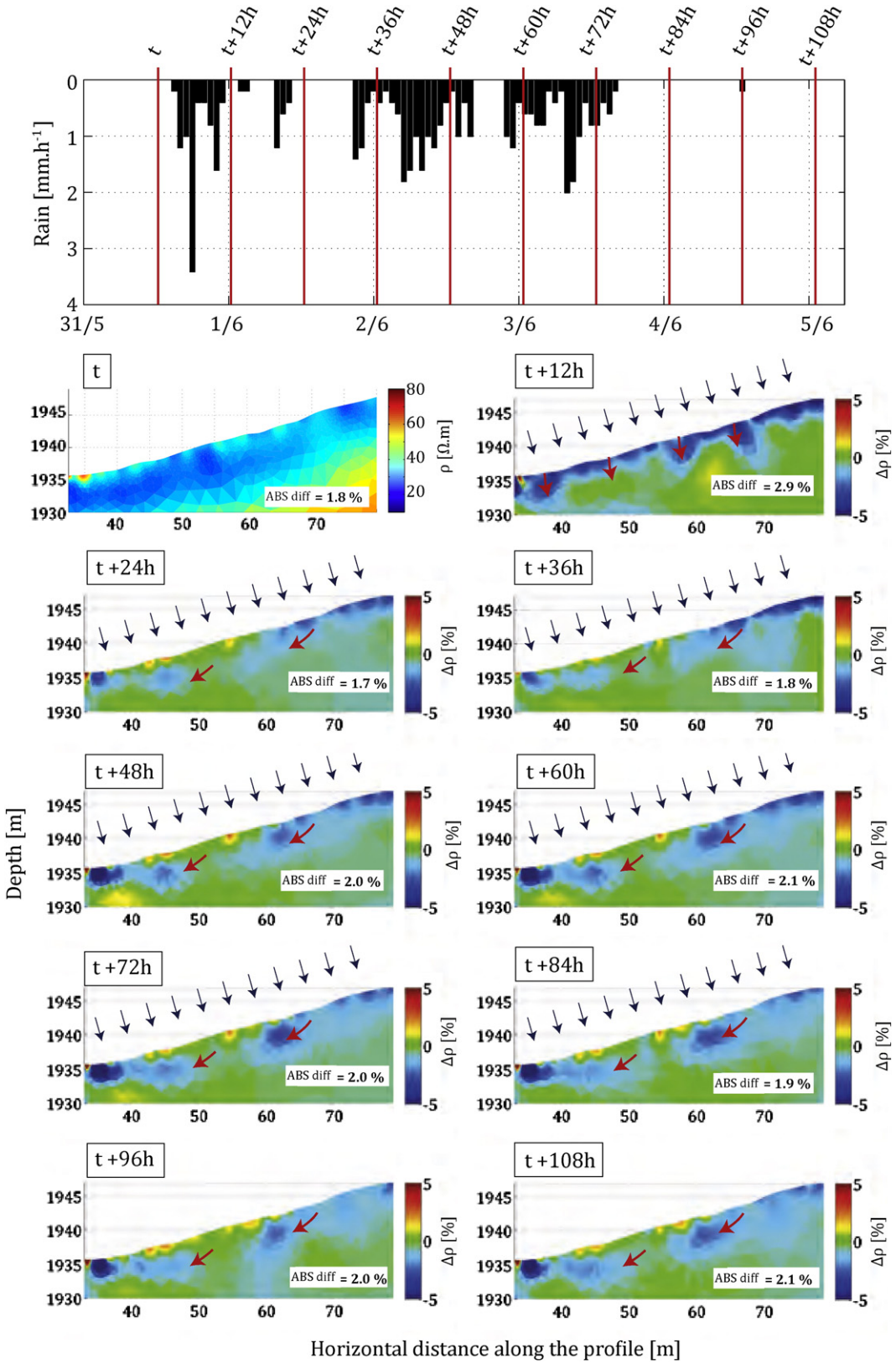

Fig. 14. Electrical response of the slope to the rainfall event R1 expressed as the percentage change of resistivity.

k_{ref} and k_T are respectively the reference and the true geometrical factors computed for the reference (first) and the current dates (t). This correction factor allows for removing the effect of the electrode movement from the resistance datasets.

A time-lapse inversion is carried out on the dataset t_1 measured the 29th of May 2011 just after the installation of the GEOMON^{4D}, using the dataset t_0 (27th of May 2011) as reference model. This time-lapse inversion is performed for the apparent resistivity computed with the raw

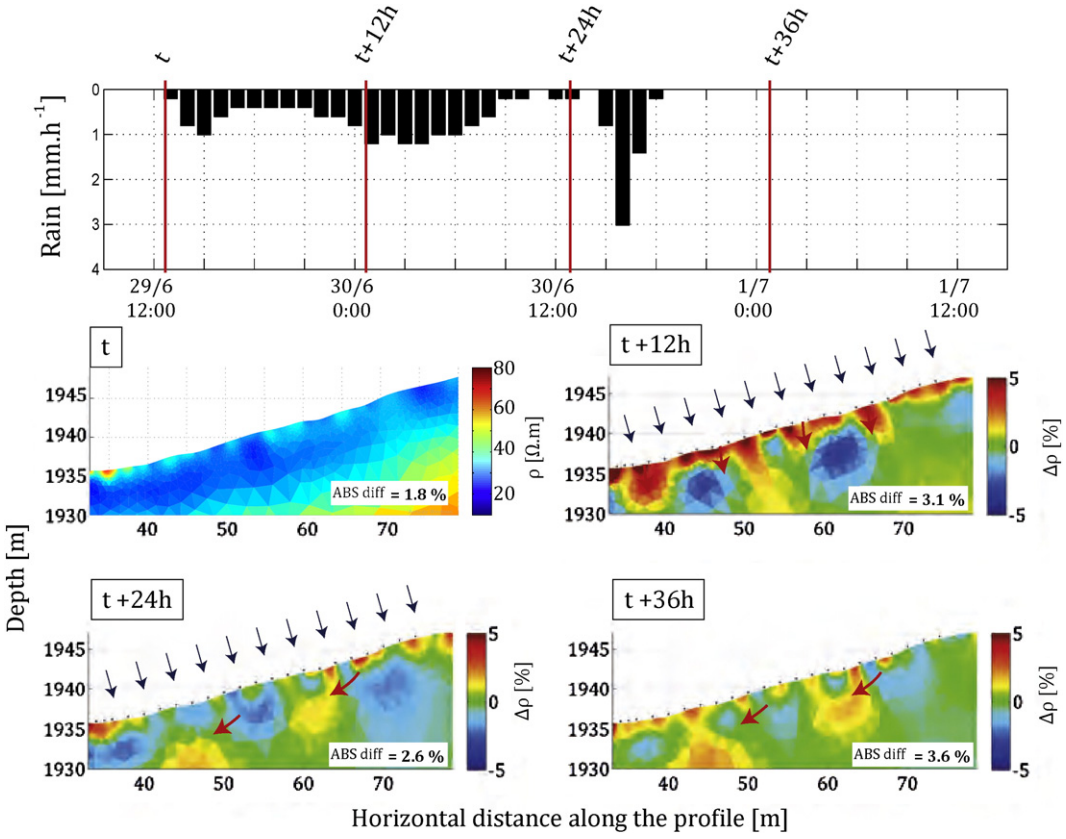

Fig. 15. Electrical response of the slope to the rainfall event R2 expressed as the percentage change of resistivity.

resistances and with the corrected resistances. The correction factor C_f is represented in Fig. 8.

The time-lapse inversion is performed using the L_2 norms on the model and the data. The RMS errors associated are respectively 1.8% and 3.3%. The percentage differences between t_1 and t_0, inverted with and without the correction, are plotted in Fig. 9. The results show large unexpected variations of resistivity for the corrected dataset (up to 15%), compared to the uncorrected dataset. These results may be explained by two reasons:

- the required accuracy on the electrode position is much lower than a few centimeters, particularly for the 0.5 and 1 m electrode spacing;
- the modeling of the topography is oversimplified in between each electrode, so that we were not able to model precisely the complex surface topography composed of several bumps and flat areas by only measuring 24 electrode positions.

  As a consequence, we decided not to correct for the electrode displacement and only to interpret the variation of resistivity for short time periods (≤5 days) with very low relative displacement rates.

3.3.3. Correction of 3D effects on 2D monitoring surveys

A strong hypothesis made in this study is the 2D assumption, inherent to 2D ERT acquisition along linear profiles. This classical practice in ERT considers that the medium is invariant in the direction perpendicular to the profile. In other words, it considers the measured apparent resistivity linked to the presence of objects located in the vertical plane passing through the profile. However, lateral conductive anomalies can deflect the current lines outside of the vertical plane and possibly result in deep (non-existent) conductive anomalies and high data misfit in the inverted tomography (Panissod et al., 2001; Dahlin, 1996). In this case, when the 3D soil electrical resistivity distribution is unknown, 3D effects are assessed by numerical modeling from a 3D resistivity model (Panissod et al., 2001). The first step of the correction therefore consists in the construction of a 3D model of resistivity covering the investigated slope. Eight 2D ERT measurements, gridding the area around the GEOMON^{4D} profile, have been acquired. The longitudinal profiles have been measured with 96 electrodes regularly spaced of 1.5 m. The 5 transversal profiles have been measured with 48 electrodes regularly spaced of 1 m. The resistivity arrays used are both dipole–dipole and Wenner–Schlumberger for each profile. Measurements characterized by voltages lower than 0.5 mV, negative resistances and standard deviations greater than 5% have been removed from the datasets.

The strategy adopted to construct the 3D model of soil resistivity consists in inverting each 2D profile and in interpolating the soil resistivity. We inverted each profile with RES2DINV (Loke and Barker, 1996) using the L_2 norm and a smoothness-constrain inversion method. The RMS errors are indicated in Table 1 and vary around 5%.

From the eight tomographies presented in Fig. 10a, we interpolated the resistivity in a pseudo 3D model characterized by voxels of 1 m^3 using an inverse distance algorithm. The exponent of the inverse distance weighting function is 1.7 and the interpolation smoothing factor is 2.35. The 3D model presents resistivity values ranging between 20 and 117 Ω · m. The model is in agreement with previous knowledge of the landslide geometry with the presence of a crest in the lower part of the profile (Gance et al., 2012; Travelletti and Malet, 2012). The shape of the bedrock is globally recovered for a threshold value equal to 50 Ω · m in agreement with the one used by Travelletti and Malet (2012).

To assess the 3D effects on the 2D monitoring profile, we compared the apparent resistivities calculated on a 3D model of resistivity with the ones of the 2D model extracted from the 3D model (Fig. 10b. A 3D mesh is created with the DC forward Finite-Element code BERT (Rücker et al.,

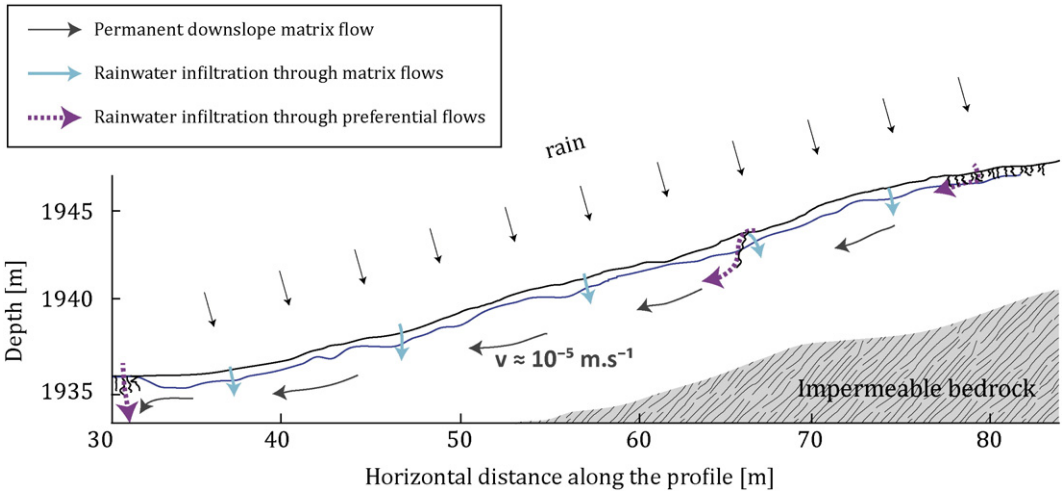

Fig. 16. Conceptual model of rainwater percolation.

2006). The electrical resistivity values were interpolated from the 3D model on a 120 × 50 × 60 m mesh. A resistivity of 100 Ω · m is assigned to the cells outside of the 3D model corresponding to resistivity values close to the ones of the substratum. By using the GEOMON^{4D} electrode positions, we compute the apparent resistivity on the 3D model of resistivity, and on the 2D profile of resistivity extracted from the 3D model. The apparent resistivity pseudo-sections and their relative differences are presented in Fig. 10c, d and e.

As expected, the largest differences between 2D and 3D models are observed for large pseudo-depths (e.g. large quadrupoles) where apparent resistivity differences rise up to 12%. Therefore, to constrain the 3D effects, we remove all the data with pseudo-depths greater than 9 m.

3.3.4. Quality of the inversion

We compared the inversion results of the raw dataset and of the corrected dataset for a randomly selected date (2nd of July 2011 at 13:00 h). The corrected dataset contains 70% of the initial 4300 measurements. The RMS errors of the, respectively, corrected and raw datasets, are 2.05% and 43.7% while the χ^2 value are respectively 0.9 and 32.4. The χ^2 value is the function minimized by the BERT2 inversion code. Its is calculated according to Eq. (3), where n is the number of data d, $f(m)$ the data calculated according the model m and ϵ the measurement error. The results of the inversion are presented in Fig. 11 and show a smoother inverted model after correction of the raw resistances.

$$\chi^2 = \frac{1}{n}\sum_{i=1}^{n}\frac{(d-i-f_i(m))^2}{\epsilon_i^2}. \quad (3)$$

Table 2
Rainfall event characteristics.

Event	Cumulated rainfall [mm]	Cumulated antecedent rainfall (10 days) [mm]	Mean intensity [mm h $^{-1}$]	Duration [h]
1	3.5	0.0	1.2	3
2	40.1	3.5	0.8	53
3	36.4	43.6	0.8	44
4	6.0	12.5	0.2	28
5	14.2	4.0	0.8	17
6	2.1	0.8	0.7	3
7	4.1	2.9	0.3	14
8	14.0	1.1	1.1	10
9	127.3	44.3	1.8	78

3.4. Inversion strategy and correction of the inverse resistivity data

3.4.1. Resistivity inversion

We used the time-lapse inversion strategy implemented in the BERT code (Günther et al., 2006). To ensure the convergence towards a realistic model, we first create a specific reference model from the highest quality subset of the corrected dataset, from the 4 to the 29 April 2012. This subset is characterized by a low percentage of data removal over the whole measurement period (<0.5%) and by a low variability of apparent resistivity over the whole measurement period (90% of the data shows a variation lower than 2% over a three day period). During this period, the soil is covered by snow. The daily temperature variations are therefore not detectable in the soil and do not affect the apparent resistivity. Finally, the total displacement observed along the sliding direction (to the North) by the GNSS antenna located on the profile is limited to 3 cm; this displacement is relatively low compared to the typical displacement rates of the landslide ranging between 0.01 and 0.03 m day $^{-1}$ (Travelletti et al., 2012a).

We first invert independently each dataset for this subset and compute the reference model as the median of the 43 inverted tomograms (acquired from 4 to 29 April, Fig. 12a). The relatively low

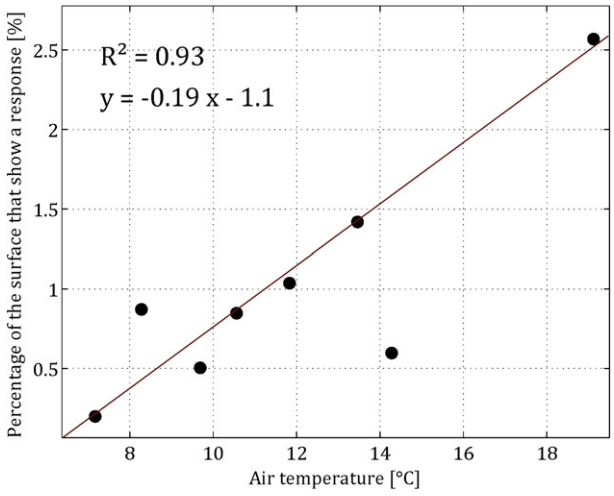

Fig. 17. Effect of air temperature (measured before a rainfall event) on the surface of the tomogram that is affected by a decrease of resistivity lower than −5%.

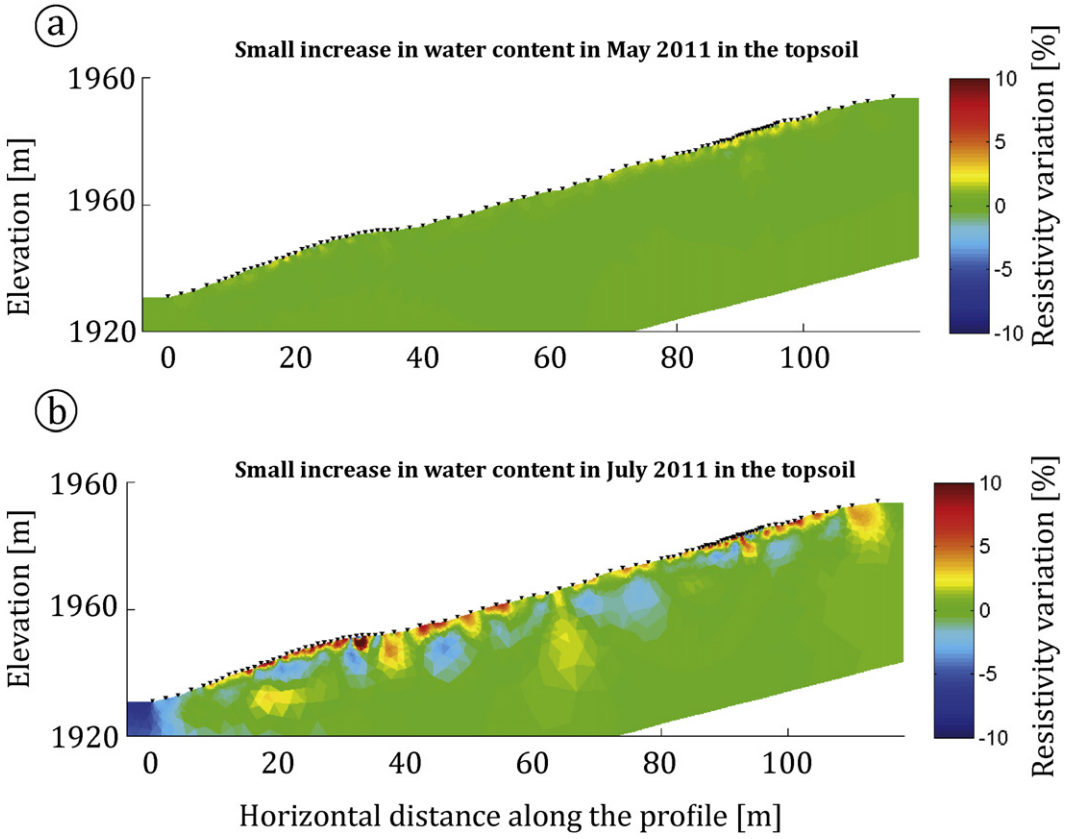

Fig. 18. Soil cooling effect by rain water. The percentage change of soil electrical resistivity after a small rainfall event could be linked to the difference between rain and initial soil temperature. Percentage change of resistivity after a cumulated rainfall amount of a) 3.5 mm in May 2011 and b) 4.1 mm in July 2011.

variation of resistivity during the period is plotted in Fig. 12b representing the maximal relative amplitude of variation *MRAV*, calculated with Eq. (4). A Maximum Relative Amplitude of Variation (MRAV) of 15% is observed at very shallow depths under the sub-area characterized by an electrode spacing of 0.5 m. Everywhere else in the tomogram, the MRAV is lower than 5%.

$$MRAV = 100 \times \frac{[max(\rho) - min(\rho)]}{median(\rho)} \quad (4)$$

Then, a time-lapse inversion of the entire dataset is carried out with the same reference model m^{ref}. The L_1 norm is used on the data and to constrain the time-lapse inversion. The L_2 norm is used on the model parameters. The time-lapse inversion is performed using the difference inversion of LaBrecque and Yang (2001). With this option, the data d^k of k th frame is corrected by the misfit of the first frame (d ^{ref}) such that $\|d^k - f(m^k) - d^{ref} + f(m^{ref})\|$ is minimized next to the regularization of the model difference $m^k - m^{ref}$.

Following Günther et al. (2006), we assume that the measurement errors are composed of a fixed percentage of errors (3%) and of an error on the voltage measurement taken as the difference between forward and reverse measurements.

3.4.2. Sensitivity of the inverted tomograms

To identify the areas of the tomogram which are constrained during the inversion, we present the sensitivity of the inversion. The sensitivity $J = \partial U/\partial \rho$ defines the contribution of each calculation cell to the result of the forward problem (voltage modeling). The log $_{10}$ of the sensitivity (Fig. 13) is in the range between −1.1 and +3.7 indicating, from our experience, a relatively good coverage of the tomogram due to the large number of measurements performed at each acquisition.

We consider arbitrarily that areas characterized by a sensitivity lower than 1 (or a log $_{10}$ of sensitivity lower than 0) are not enough covered to be considered for the interpretation. The limit associated with this threshold is located just above the interface between the bedrock and the landslide material.

3.4.3. Correction of the inverted resistivity from the effects of ground water temperature and conductivity

We correct the inverted resistivity for ground water conductivity changes assuming a linear dependence between soil resistivity and water resistivity (Archie type law, Archie, 1942) and where the effect of clay surface conductivity is accounted by applying a fixed coefficient β. The resistivity is corrected for a reference conductivity C_{ref} of 2.0 mS cm $^{-1}$. The resistivity corrected from the conductivity variations ρ_{c1} is therefore computed according to Eq. (5) where β is a coefficient accounting for the effect of surface conductivity of clay particle equal to 0.2 and computed from the difference of resistivity between two measurements with different ground water conductivity and identical temperature$\rho(t)$ is the raw inverted resistivity and $C(t)$ the ground water conductivity measured at 1 m of depth.

$$\rho_{c1} = \beta\rho(t)\frac{C_{ref}}{C(t)} \quad (5)$$

The effect of soil temperature is corrected by using the Campbell model (Campbell et al., 1948) with a temperature slope gradient α equal to 0.023 C $^{-1}$ also used by Travelletti et al. (2012b) for black marls soils. The corrected resistivity is computed for a reference

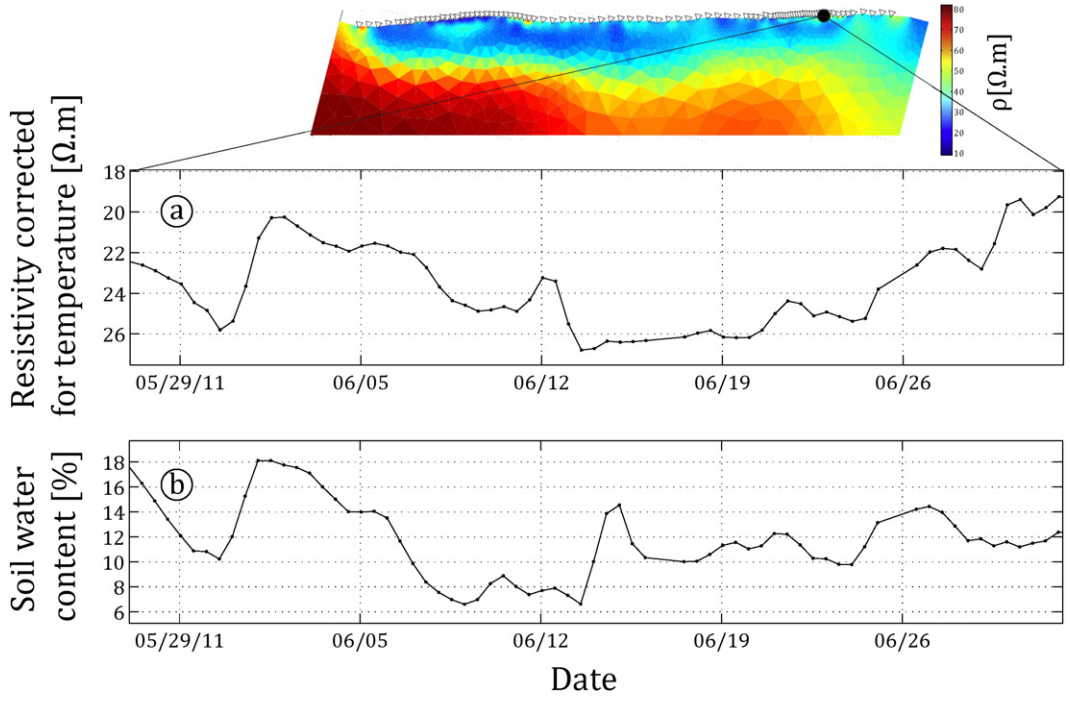

Fig. 19. Correlation between electrical resistivity corrected from soil surface temperature variation with the measured soil water content: a) resistivity corrected from soil temperature measurements and b) soil water content. The soil temperature, water content and electrical resistivity are measured at the same place and at −0.1 m in depth.

temperature T_{ref} equal to 25 °C. The resistivity corrected from the conductivity variations ρ_{c2} is therefore computed according to Eq. (6) where $\rho(t)$ is the raw inverted resistivity and T the groundwater temperature measured at 1 m of depth.

$$\rho_{c2} = \rho(t)\frac{1}{1+\alpha(T-T_{ref})} \tag{6}$$

4. Interpretation of the electrical responses of the slope to rainfall events

We assume that, with the corrections applied, the effects of the non-hydrological factors on the resistivity variations is limited as much as possible. We select two significant rainfall events (R1, R2) to interpret the electrical responses of the slope. The rainfall event R1 is a relatively large rainfall event starting on 31 May 2011 when the groundwater

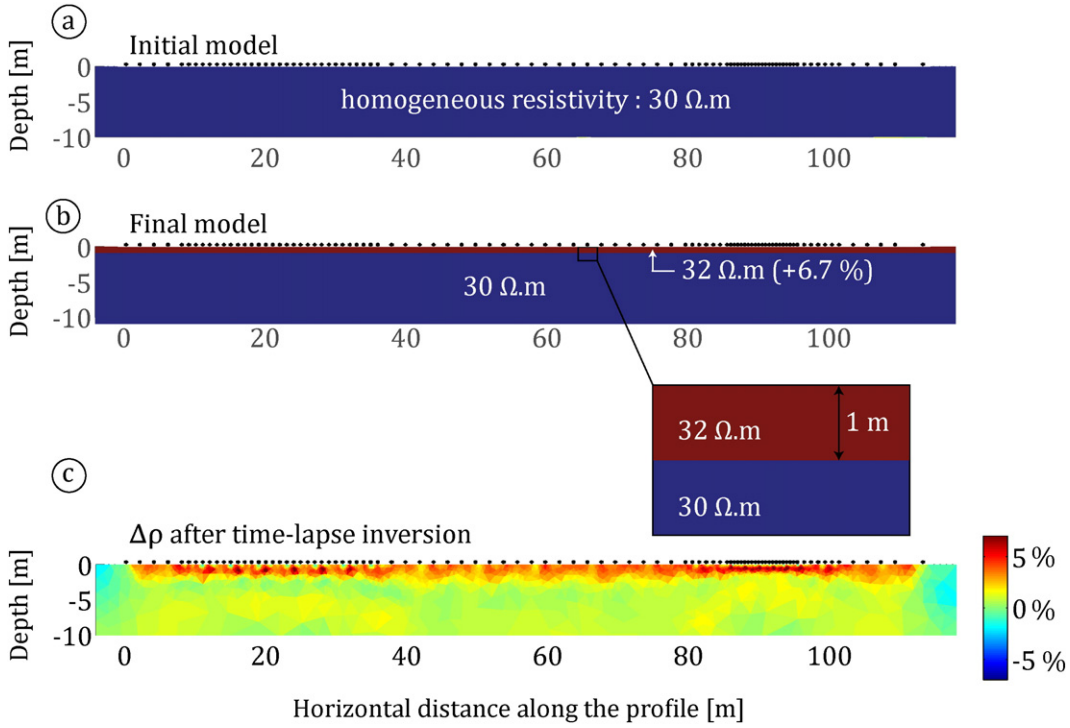

Fig. 20. Analysis of the effect of sensitivity change of the device due to the cooling of the infiltrating water in the vadose zone.

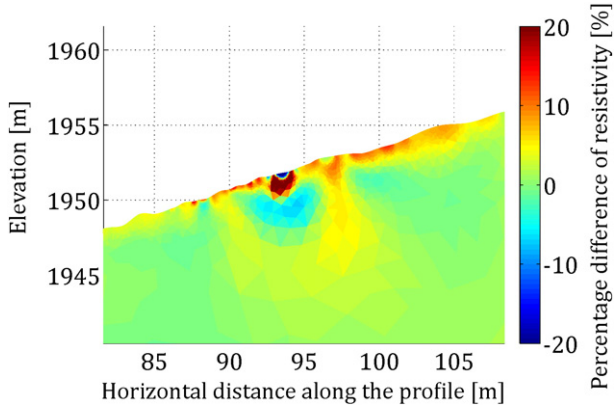

Fig. 21. Example of typical inversion artifact caused by surface fissures, observed in the low fissure density unit with an inter-electrode spacing of 0.5 m the 2nd of June 2011.

table ends rising (0.5 m of depth). The total rain amount was 40.1 mm, the duration was 53 h, and the mean intensity was 0.8 mm h^{-1}. The initial degree of saturation of the soil was low (3.5 mm of cumulated rainfall over the past 10 days). The air temperature and the soil temperature at the surface were around 12 °C. The electrical response associated with R1 lasts for 4.5 days and is relatively smoothed in time. The electrical response for the 2 m inter-electrode spacing unit (non-fissured unit, less affected by inversion artifacts and by electrode differential movement) is presented in Fig. 14 in terms of relative percentage change of resistivity compared to the date *t* (before the start of the rainfall event). The electrical response is globally weak (≈5%) and can be divided into two periods. First, a decrease of resistivity at shallow depth (at t + 12 h) is observed. At t + 24 h, this anomaly is not visible anymore and the variation of electrical resistivity is more visible in depth where a conductive anomaly is developing and is moving downslope at a velocity of approximately 5 m in 2.5 days, with an approximate speed of 2.10^{-5} m s^{-1} in agreement with the soil permeability values measured for this unit and ranging between 10^{-4} and 10^{-6} m s^{-1} (Malet and Maquaire, 2004).

Qualitatively, we can interpret this decrease of resistivity to an increase of the soil water content. However, the major part of the electrical response after t + 24 h is located below the groundwater table where no electrical resistivity variation is expected. Because the rainwater conductivity is very low compared to the ground water, we do not expect that the rain water infiltration induces a decrease of resistivity. We thus interpret these variations as the result of heat exchanges between the rainwater, the vadose zone water and the groundwater. The decrease of resistivity at shallow depths at t + 12 h is interpreted as a real increase of soil water content in the vadose zone, also measured by the soil water probes. At t + 24 h, the stable measured soil water content and the increase of resistivity at shallow depths is explained by the progressive warming of the infiltrated rain water by the soil. From t + 24 h to t + 108 h, the conductive anomaly located below the groundwater table and moving progressively downslope is interpreted as the percolation of a mass of warm (≥2 °C) water permanently supplied by a fissure network located upslope. This interpretation is in agreement with the low temperature of the groundwater table observed for this period (≈2 °C) that is certainly lower than the rainwater temperature. Although a large number of hydrological observations are available, there are no measurements that support our hypothesis for explaining the electrical response of the slope. No significant temperature variations of the groundwater are observed at that period. The electrical response patterns for the different rainfall events strengthen nevertheless our hypothesis. For example, we show the electrical response of the rainfall event R2 occurring one month later when the groundwater temperature is higher (≈12 °C).

The rainfall event R2 is starting on 29 June 2011 at a period when the groundwater table level is lower (0.68 m of depth). The total amount of rain of the event is 14.2 mm, the duration is 17 h, for a mean intensity of 0.8 mm h^{-1}. The initial degree of saturation of the soil is low (4.0 mm of cumulated rainfall over the past 10 days). The air and soil temperature are around 20 °C. The electrical response consecutive to this rainfall event is short (1.5 days). The electrical response for the 2 m inter-electrode spacing unit (non-fissured unit, less affected by inversion artifacts and electrode differential movement) is presented in Fig. 15.

The infiltration of a cold rainwater in the vadose zone induces a 5% increase of resistivity at t + 12 h. At t + 24 h, the shallow resistive anomaly disappears indicating that the water temperature equilibrates with the soil temperature. The fluxes of warm water in the saturated zone create conductive anomalies. The presence of residual resistive anomalies located upslope in the surface is interpreted as the presence of cold water fluxes under the groundwater table continuously supplied by the fissure network located upslope. At t + 36 h, the amplitude of resistivity variations is very low. The amount of infiltrated rainwater is not sufficient to sustainably cool the groundwater temperature.

On the basis of these observations, a simple conceptual model of rainwater percolation is proposed in Fig. 16. First, rainwater percolates vertically by matrix flow. The topsoil can be cooled or warmed during the percolation and the temperature of the infiltrated water tends progressively to reach the soil temperature. Second, the fissure network that is draining the surface waters by runoff acts as a direct preferential flowpath to the groundwater.

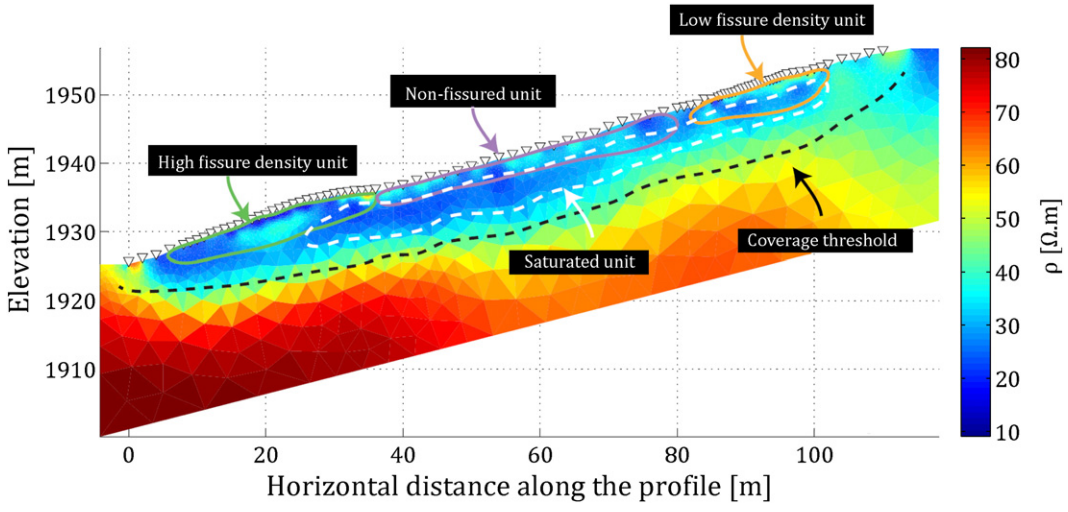

Fig. 22. Definition of the different spatial units used to analyze separately the inverted resistivity electrical responses of the slope.

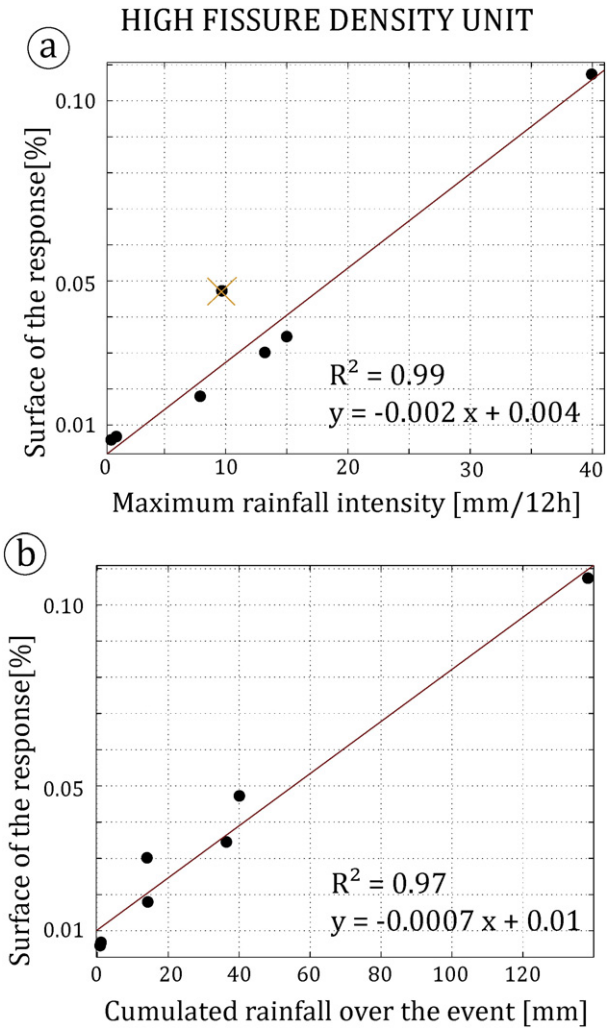

Fig. 23. Relation between the percentage of the surface of response and a) the maximal rainfall intensity (The black point deleted with a red cross considered as an outlier has not been used for the linear regression) and b) the cumulated rainfall per event in the highly-fissured unit.

5. Effect of heat exchanges between rainwater, vadose zone water and groundwater

The analysis of the electrical responses to rainfall events demonstrates the main contribution of thermal effects over hydrological effects on the resistivity variations. The thermal signal is the result of a complex combination of heat exchanges between the rainwater, the soil water, the groundwater and the solid particles. The effect of air temperature is statistically visible on the electrical response. During the monitoring period, we identified nine rainfall events which characteristics are indicated in Table 2. Fig. 17 presents the percentage of the surface of the tomogram with a decrease of resistivity lower than −5%. This surface is larger when the air temperature is higher. Assuming that the rainwater temperature is correlated to the air temperature, this result shows that the more the rainwater infiltrated is warm, the more the conductive anomaly in the tomogram is large, possibly due to a stronger warming of a part of the ground water table.

Fig. 18 presents two very different electrical responses to a slight humidification of the soil not corrected from temperature variations. It also illustrates the impact of air and soil temperatures. Fig. 18a and b respectively show the relative variation of soil resistivity after two equivalent rainfall events characterized by a total amount of water equal to 3.5 mm and 4.1 mm (events 1 and 7 of Table 2), respectively occurring in May and July 2011.

In this context, the correction of the surface temperatures could allow for the study of the real hydrological signal. Fig. 19 shows a relatively good correlation of the corrected resistivity (using soil temperature measured at −0.1 m in depth and the Campbell model) with the soil water content recorded at −0.1 m in depth, thus indicating a good accuracy of the topsoil temperature correction. It remains however difficult to correct for the effect of temperature the entire tomogram. This difficulty lies in the soil heterogeneity that result in a highly heterogeneous spatial distribution of the hydrological parameters (e.g. ground water table depth, soil moisture) and soil temperature. A total correction of the temperature effect on the electrical resistivity would therefore require spatially distributed measurements of the soil temperature and hydrology.

6. Discussion

The resistivity changes observed in this study are weak due to the large clay fraction of the soil. The effects of some non-hydrological factors could not be corrected neither on the raw data, nor on the inverted resistivity. We further describe and discuss their possible effects.

6.1. Sensitivity of the device

In ERT monitoring studies, the distribution of sensitivity changes with the temporal change of the distribution of soil resistivity. In this context, we can observe resistivity variations in depth that only result from a change of sensitivity due to true resistivity variation at shallower depths. Depending on the electrode spacing and on the soil resistivity distribution, a variation of actual resistivity in shallow layers can lead to an opposite variation of apparent resistivity at intermediate electrode spacing (Descloitres et al., 2008; Kunetz, 1966). The distribution and amplitude of this effect can be assessed numerically (Clément et al., 2009).

In this context, we model the effect of the warming of the infiltrating rainwater in the vadose zone on a synthetic model. The initial model is a flat homogeneous resistivity model (30 Ω · m, Fig. 20a). In the final model, we model the vadose zone as a layer of 1 m of thickness. To reproduce the cooling of the infiltrating water in the vadose zone, we slightly increase the resistivity of this layer from 30 to 32 Ω · m (increase of 7%, Fig. 20b). For both models, synthetic dataset are first generated with BERT for each model and the datasets are inverted using the same options than for the real dataset inversions using a time-lapse approach.

The time-lapse inversion of the calculated dataset allows for reproducing the +7% increase of resistivity at the surface (particularly in the 0.5 and 1.0 m electrode spacing units). This increase of resistivity at shallow depths results in a 1–2% increase of resistivity between 5 and 10 m of depth. These inversionartifacts are small in amplitudes but are relatively high in comparison to the resistivity variations observed at Super-Sauze. They constitute a supplementary difficulty for the study of water infiltration in the vadose zone in clayey soils.

6.2. Spatial heterogeneity of the soil surface

Another phenomenon able to produce inversion artifacts in the inverted tomograms is related to the high sensitivity of ERT to the spatial heterogeneity of the soil surface and more particularly to the surface fissures. The current inversion algorithms cannot reproduce the sharp variation of resistivity produced by the presence of a surface fissure. It finally results in large inversion artifacts in the vicinity of the heterogeneity which sizes vary with the presence/absence of water inside the fissures, the closing/opening of the fissures with the landslide movement and possible decrease of the coupling between the soil and the electrodes. This complex problem, described in Gance et al. (2015), is

responsible of inversion artifacts like the one presented in Fig. 21 in the 0.5 m inter-electrode spacing unit, certainly created by the filling of the fissure by water. Gance et al. (2015) propose a methodology to attenuate these artifacts but it requires a good knowledge of the fissure geometry and is therefore not applicable for long-term experiments, for which the fissure geometry constantly evolves in space and time.

6.3. Statistical relationships between electrical responses of the slope and slope hydrology

The strong effect of heat exchanges between rainwater, soil water in the vadose zone and groundwater and the effects of sensitivity changes and surface heterogeneities prevent us from extracting reliable statistical relationships between the electrical response of the slope and the hydrological observations. To minimize the inversion artifacts, we computed several electrical responses consecutive to the rainfall events (area of the response, median, mean and quantiles) for five different units defined according to the inter-electrode spacing, the fissure size and the fissure density (Fig. 22). The relationships with meteorological parameters globally show larger electrical responses (expressed in terms of relative surface of the calculation cells with a decrease of resistivity lower than −5%) for larger rainfall events (Fig. 23). The small number of rainfall events and our difficulty to obtain hydrological and temperature measurements on the long-term for this complex monitoring site were obstacles for a quantitative interpretation of the datasets.

7. Conclusion

With the idea to improve our understanding of the hydrological behavior of the Super-Sauze clayey landslide, we installed for one year the GEOMON^{4D} device for monitoring the soil electrical resistivity two times per day along a longitudinal profile. A processing methodology is proposed to interpret long-term resistivity datasets by correcting the effects of non-hydrological factors on the observations. We limited the 3D effects by numerical simulations on a 3D resistivity model of the area. We reduced the effect of the differential electrode movement on the resistivity variation by measuring the electrode displacement with stereo-photogrammetry. We proposed a methodology to filter the erroneous measurements from the dataset and a methodology of time-lapse inversion based on the use of a fixed reference model computed on a period with stable resistivity values. The inverted resistivity are corrected for groundwater conductivity and temperature variations.

Then, by interpreting the electrical responses of the slope to two rainfall events, we showed the strong effect of heat exchanges between the groundwater, the soil water in the vadose zone and the rainwater that hide the variations of resistivity due to a variation of the soil water content. We demonstrate that despite the absence of information on the soil water content and the soil temperature in the vadose zone, the sensitivity of ERT to temperature variation allows for imaging water fluxes in the saturated zone and to highlight the existence of both matrix and preferential flows that do not occur at the same time and for the same duration. From the electrical response of the slope, we propose a conceptual model of infiltration of the rainwater in the subsoil through matrix and preferential flows. Despite this enhancement in data quality before and after inversion, we were not able to define any statistical relationships between the electrical response of the slope and the landslide hydrology.

The conclusion of this study is that more attention should be paid to the possible thermal exchanges between the rainwater, the soil water and, the groundwater for the interpretation of long-term electrical resistivity, observations, specifically for quantitative analyses of water fluxes in the vadose zone. This study demonstrates the primary effect of thermal exchanges on the hydrological effect, which is particularly for clay-rich slope material. Similar effects could also be observed for slopes where the hydrological effect is dominant preventing from an accurate quantification of soil water content variations.

In these conditions, the advanced processing of time-lapse ERT datasets does not allow for being sensitive to water exchanges in the vadose zone without a distributed measurement of soil temperature, in-situ measurements of resistivity and laboratory measurements of the clay surface conductivity. Perspectives of improvement are the simultaneous measurements of resistivity and temperature (at the surface and in depth) and their interpretation through coupled hydro-thermo-electrical models. Such study would allow not only imaging the water exchanges in the vadose zone but also in the saturated zone.

Acknowledgement

This work is part of the French Landslide Observatory OMIV (Observatoire Multi-disciplinaire des instabilités de versants) and has been financially supported by the BRGM Carnot Institute, the project CRITEX – Challenging equipment for the spatial and temporal exploration of the critical zone – funded by the French Research Agency (ANR)-11-EQPX-0011 in the frame of the EquipEX program, and the project TEMPEL Temporal changes of geoelectrical properties as possible indicator of future failure of high risk landslides -, funded by the Austrian Science Fund (FWF)-TRP 175-N21 in frame of the Translational Brainpower Program. The authors would like to thank Marc Descloîtres (LTHE, Grenoble) and Denis Jongmans (ISTerre, Grenoble) for constructive comments and discussions on the data processing and interpretation. We further acknowledge Thomas Günther (LIAG, Hanover) for providing the BERT inversion code and associated usage tips.

References

Archie, G., 1942. The electrical resistivity log as an aid in determining some reservoir characteristics. Trans. AIME 146, 54–62.
Arora, T., Ahmed, S., 2011. Characterization of recharge through complex vadose zone of a granitic aquifer by time-lapse electrical resistivity tomography. J. Appl. Geophys. 73, 35–44.
Bhattacharya, B., Dutta, I., 1982. Depth of investigation studies for gradient arrays over homogeneous isotropic half-space. Geophysics 47, 1198–1203.
Bièvre, G., Jongmans, D., Winiarski, T., Zumbo, V., 2012. Application of geophysical measurements for assessing the role of fissures in water infiltration within a clay landslide (Trièves area, French Alps). Hydrol. Process. 26, 2128–2142.
Bogaard, T., Van Asch, T.W., 2002. The role of the soil moisture balance in the unsaturated zone on movement and stability of the Beline landslide, France. Earth Surf. Process. Landf. 27, 1177–1188.
Campbell, R., Bower, C., Richards, L., 1948. Change of electrical conductivity with temperature and the relation of osmotic pressure to electrical conductivity and ion concentration for soil extracts. Soil Sci. Soc. Am. Proc. 13, 66–69.
Chambers, J., Gunn, D., Wilkinson, P., Meldrum, P., Haslam, E., Holyoake, S., Kirkham, M., Kuras, O., Merritt, A., Wragg, J., 2014. 4d electrical resistivity tomography monitoring of soil moisture dynamics in an operational railway embankment. Near Surf. Geophys. 12, 61–72.
Clément, R., Descloitres, M., Günther, T., Ribolzi, O., Legchenko, A., 2009. Influence of shallow infiltration on time-lapse ERT: experience of advanced interpretation. Compt. Rendus Geosci. 341, 886–898.
Dahlin, T., 1996. 2d resistivity surveying for environmental and engineering applications. First Break 14.
Dahlin, T., Zhou, B., 2004. A numerical comparison of 2d resistivity imaging with 10 electrode arrays. Geophys. Prospect. 52, 379–398.
Dahlin, T., Zhou, B., 2006. Multiple-gradient array measurements for multichannel 2d resistivity imaging. Near Surf. Geophys. 4, 113–123.
Debieche, T.H., Bogaard, T.A., Marc, V., Emblanch, C., Krzeminska, D.M., Malet, J.P., 2012. Hydrological and hydrochemical processes observed during a large-scale infiltration experiment at the Super-Sauze mudslide (France). Hydrol. Process. 26, 2157–2170.
Descloitres, M., Ruiz, L., Sekhar, M., Legchenko, A., Braun, J.J., Mohan Kumar, M.S., Subramanian, S., 2008. Characterization of seasonal local recharge using electrical resistivity tomography and magnetic resonance sounding. Hydrol. Process. 22, 384–394.
Gance, J., Grandjean, G., Samyn, K., Malet, J.P., 2012. Quasi-newton inversion of seismic first arrivals using source finite bandwidth assumption: application to subsurface characterization of landslides. J. Appl. Geophys. 87, 94–106.
Gance, J., Malet, J.P., Dewez, T., Travelletti, J., 2014. Target detection and tracking of moving objects for characterizing landslide displacements from time-lapse terrestrial optical images. Eng. Geol. 172, 26–40.
Gance, J., Sailhac, P., Malet, J.P., 2015. Corrections of surface fissure effect on apparent resistivity measurements. Geophys. J. Int. 200, 1118–1135.
Grandjean, G., Malet, J.P., Bitri, A., Méric, O., 2007. Geophysical data fusion by fuzzy logic for imaging the mechanical behaviour of mudslides. Bull. Soc. Geol. Fr. 178, 127–136.
Grandjean, G., Pennetier, C., Bitri, A., Meric, O., Malet, J.P., 2006. Caractérisation de la structure interne et de l'état hydrique de glissements argilo-marneux par tomographie

géophysique: l'exemple du glissement-coulée de super-sauze (alpes du Sud, France). Compt. Rendus Geosci. 338, 587–595.
Günther, T., Rücker, C., Spitzer, K., 2006. Three-dimensional modelling and inversion of dc resistivity data incorporating topography—II. Inversion. Geophys. J. Int. 166, 506–517.
Hilbich, C., Fuss, C., Hauck, C., 2011. Automated time-lapse ERT for improved process analysis and monitoring of frozen ground. Permafr. Periglac. Process. 22, 306–319.
Jomard, H., Lebourg, T., Binet, S., Tric, E., Hernandez, M., 2007. Characterization of an internal slope movement structure by hydrogeophysical surveying. Terra Nova 19, 48–57.
Krzeminska, D.M., Bogaard, T.A., Malet, J.P., van Beek, L.P.H., 2013. A model of hydrological and mechanical feedbacks of preferential fissure flow in a slow-moving landslide. Hydrol. Earth Syst. Sci. 17, 947–959.
Kunetz, G., 1966. Principles of direct current resistivity prospecting. Number 1 in Geoexploration Monographs. Gebr. Borntraeger.
Kuras, O., Pritchard, J.D., Meldrum, P.I., Chambers, J.E., Wilkinson, P.B., Ogilvy, R.D., Wealthall, G.P., 2009. Monitoring hydraulic processes with automated time-lapse electrical resistivity tomography (ALERT). Compt. Rendus Geosci. 341, 868–885.
LaBrecque, D.J., Yang, X., 2001. Difference inversion of ERT data: a fast inversion method for 3-D in situ monitoring. J. Environ. Eng. Geophys. 6, 83–89.
Lebourg, T., Binet, S., Tric, E., Jomard, H., El Bedoui, S., 2005. Geophysical survey to estimate the 3d sliding surface and the 4d evolution of the water pressure on part of a deep seated landslide. Terra Nova 17, 399–406.
Lebourg, T., Hernandez, M., Zerathe, S., El Bedoui, S., Jomard, H., Fresia, B., 2010. Landslides triggered factors analysed by time lapse electrical survey and multidimensional statistical approach. Eng. Geol. 114, 238–250.
Lehmann, P., Gambazzi, F., Suski, B., Baron, L., Askarinejad, A., Springman, S.M., Holliger, K., Or, D., 2013. Evolution of soil wetting patterns preceding a hydrologically induced landslide inferred from electrical resistivity survey and point measurements of volumetric water content and pore water pressure: evolution of wetting patterns preceding a rapid landslide. Water Resour. Res. 49, 7992–8004.
Loke, M., Barker, R., 1996. Rapid least-squares inversion of apparent resistivity pseudosections by a quasi-Newton method1. Geophys. Prospect. 44, 131–152.
Luongo, R., Perrone, A., Piscitelli, S., Lapenna, V., 2012. A prototype system for time-lapse electrical resistivity tomographies. Int. J. Geophys. 2012, 1–12.
Malet, J., Maquaire, O., 2004. Hydrological behaviour of earthflows developed in clay-shales: investigation, concept and modelling. In: Picarelli, L. (Ed.), The Occurrence and Mechanisms of Flows in Natural Slopes and Earthfills. Patron Editore, Bologna, pp. 175–193.
Malet, J.P., Auzet, A.V., Maquaire, O., Ambroise, B., Descroix, L., Esteves, M., Vandervaere, J.P., Truchet, E., 2003. Soil surface characteristics influence on infiltration in black marls: application to the Super-Sauze earthflow (southern Alps, France). Earth Surf. Process. Landf. 28, 547–564.
Malet, J.P., Laigle, D., Remaître, A., Maquaire, O., 2005b. Triggering conditions and mobility of debris flows associated to complex earthflows. Geomorphology 66, 215–235.
Malet, J., Van Asch, T., Van Beek, R., Maquaire, O., et al., 2005a. Forecasting the behaviour of complex landslides with a spatially distributed hydrological model. Nat. Hazards Earth Syst. Sci. 5, 71–85.
Maquaire, O., Flageollet, J., Malet, J., Schmutz, M., Weber, D., Klotz, S., Albouy, Y., Descloîtres, M., Dietrich, M., Guérin, R., et al., 2001. Une approche multidisciplinaire pour la connaissance d'un glissement-coulée dans les marnes noires du callovien-oxfordien:(super-sauze, alpes-de-haute-provence, France). Rev. Fr. Géotech. 15–31.
Miller, C.R., Routh, P.S., Brosten, T.R., McNamara, J.P., 2008. Application of time-lapse ERT imaging to watershed characterization. Geophysics 73, G7–G17.
Montety, V.d., Marc, V., Emblanch, C., Malet, J.P., Bertrand, C., Maquaire, O., Bogaard, T., 2007. Identifying the origin of groundwater and flow processes in complex landslides affecting black marls: insights from a hydrochemical survey. Earth Surf. Process. Landf. 32, 32–48.
Panissod, C., Michot, D., Benderitter, Y., Tabbagh, A., 2001. On the effectiveness of 2d electrical inversion results: an agricultural case study. Geophys. Prospect. 49, 570–576.
Perrone, A., Lapenna, V., Piscitelli, S., 2014. Electrical resistivity tomography technique for landslide investigation: a review. Earth Sci. Rev. 135, 65–82.
Peter-Borie, 2011. Electrical resistivity monitoring with buried electrodes and cables: noise estimation with repeatability tests. Near Surf. Geophys.
Philip, J.R., 1991. Infiltration and downslope unsaturated flows in concave and convex topographies. Water Resour. Res. 27, 1041–1048.
Revil, A., Karaoulis, M., Johnson, T., Kemna, A., 2012. Review: some low-frequency electrical methods for subsurface characterization and monitoring in hydrogeology. Hydrogeol. J. 20, 617–658.
Robert, T., Caterina, D., Deceuster, J., Kaufmann, O., Nguyen, F., 2012. A salt tracer test monitored with surface ERT to detect preferential flow and transport paths in fractured/karstified limestones. Geophysics 77, B55–B67.
Rücker, C., Günther, T., Spitzer, K., 2006. Three-dimensional modelling and inversion of dc resistivity data incorporating topography — I. Modelling. Geophys. J. Int. 166, 495–505.
Stumpf, A., Malet, J.P., Kerle, N., Niethammer, U., Rothmund, S., 2013. Image-based mapping of surface fissures for the investigation of landslide dynamics. Geomorphology 186, 12–27.
Supper, R., Roemer, A., 2003. New achievements in development of a high-speed geoelectrical monitoring system for landslide monitoring. Proceedings of the EEGS, 9th meeting, Prag.
Supper, R., Roemer, A., 2004. New achievements in development of a high-speed geoelectrical monitoring system for landslide monitoring (GEOMONITOR2d). Proceedings of SAGEEP 2004 meeting, Colorado Springs, p. 556.
Supper, R., Ottowitz, D., Jochum, B., Kim, J.H., Römer, A., Baron, I., Pfeiler, S., Lovisolo, M., Gruber, S., Vecchiotti, F., 2014. Geoelectrical monitoring: an innovative method to supplement landslide surveillance and early warning. Near Surf. Geophys. 12, 133–150.
Supper, R., Romer, A., Hübl, G., 2002. Development of a new, fast remote controlled 3d geoelectrical system for subsurface surveillance. Proceedings of the EEGS, 8th Meeting, Aveiro, Portugal.
Supper, R., Römer, A., Jochum, B., Bieber, G., Jaritz, W., 2008. A complex geo-scientific strategy for landslide hazard mitigation—from airborne mapping to ground monitoring. Adv. Geosci. 14.
Tabbagh, J., Samouëlian, A., Tabbagh, A., Cousin, I., 2007. Numerical modelling of direct current electrical resistivity for the characterisation of cracks in soils. J. Appl. Geophys. 62, 313–323.
Travelletti, J., Malet, J.P., 2012. Characterization of the 3d geometry of flow-like landslides: a methodology based on the integration of heterogeneous multi-source data. Eng. Geol. 128, 30–48.
Travelletti, J., Delacourt, C., Allemand, P., Malet, J., Schmittbuhl, J., Toussaint, R., Bastard, M., 2012a. Correlation of multi-temporal ground-based optical images for landslide monitoring: application, potential and limitations. ISPRS J. Photogramm. Remote Sens. 70, 39–55.
Travelletti, J., Sailhac, P., Malet, J.P., Grandjean, G., Ponton, J., 2012b. Hydrological response of weathered clay-shale slopes: water infiltration monitoring with time-lapse electrical resistivity tomography. Hydrol. Process. 26, 2106–2119.
Uhlemann, S., Wilkinson, P.B., Chambers, J.E., Maurer, H., Merritt, A.J., Gunn, D.A., Meldrum, P.I., 2015. Interpolation of landslide movements to improve the accuracy of 4d geoelectrical monitoring. J. Appl. Geophys. 121, 93–105.
Van Asch, T., Buma, J., 1997. Modelling groundwater fluctuations and the frequency of movement of a landslide in the Terres Noires region of Barcelonnette (France). Earth Surf. Process. Landf. 22, 131–141.
Van Asch, T., Buma, J., Van Beek, L., 1999. A view on some hydrological triggering systems in landslides. Geomorphology 30, 25–32.
Wilkinson, P.B., Chambers, J.E., Meldrum, P.I., Gunn, D.A., Ogilvy, R.D., Kuras, O., 2010. Predicting the movements of permanently installed electrodes on an active landslide using time-lapse geoelectrical resistivity data only. Geophys. J. Int. 183, 543–556.